CAVITIES WITH A SWING

A. Schnase
Jülich Research Centre, Jülich, Germany

Abstract
A description is given of the basic configurations used in variable frequency accelerating cavities and drift tubes that use ferrite. The relevant ferrite parameters that determine cavity performance are discussed. Equivalent circuits for the load on the RF power source and the ferrite biasing source are given. New aspects are cavities filled with amorphous alloys that show broadband behaviour without tuning loops. This text is a rewritten and updated version of 'Ferrite dominated cavities' by I.S.K. Gardner [1].

1. INTRODUCTION

Ferrite cavities are the devices that transfer energy to the beam in proton and ion synchrotrons. The particle velocity starts from the non-relativistic region and may reach the relativistic region. Depending on the circumference of the machine and the harmonic used, the frequency swing is within the approximate range of 10 kHz to 10 MHz. A simplified structure of an RF system is shown in Fig. 1. An oscillator generates a frequency derived from the radial beam position and actual dipole field. The signal is amplified and drives a cavity, where the beam sees the acceleration voltage.

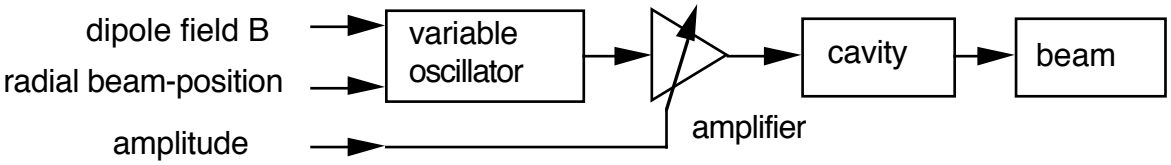

Fig. 1: Simplified structure of an RF system

To create the acceleration voltage along the beam pipe, a gap is inserted (see Fig. 2(a)). This device will radiate, so screening is necessary (see Fig. 2(b)). The outer shielding is a short circuit for the acceleration voltage, so it is inductively isolated from the gap by the use of ferrites (see Fig. 2(c)). Then the inductance, L, of the ferrite combined with the capacitance, C, of the gap forms a resonant circuit, whose frequency has to be tuned to the velocity of the circulating beam.

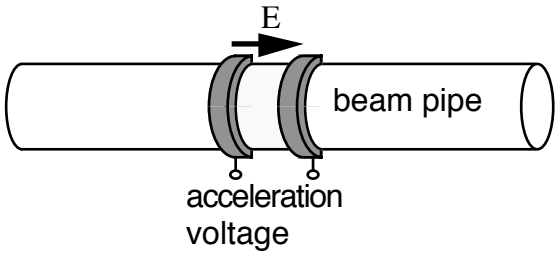

Fig. 2(a): Insertion of an isolating gap into the beam pipe to create a connection for the acceleration voltage

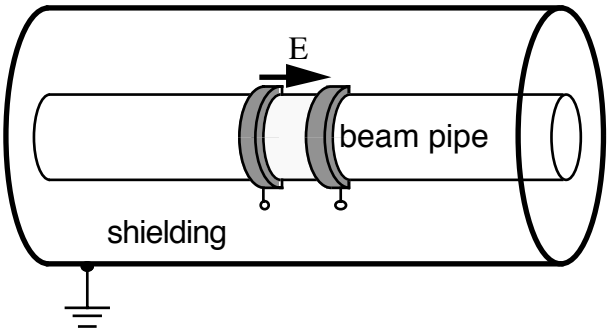

Fig. 2(b): Screening against RF radiation

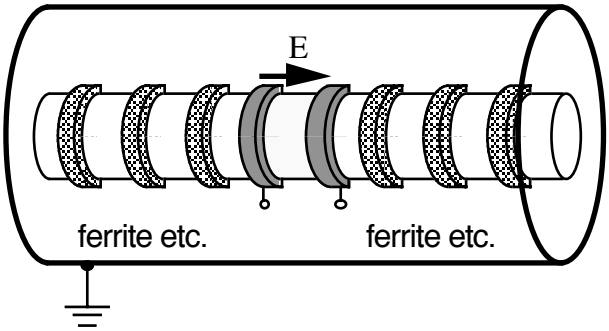

Fig. 2(c): Inductive isolation of the acceleration gap from the beam pipe and outer shielding

An incomplete list of ferrite-filled accelerating structures used in accelerators is given in Table 1. The ferrites for these systems are supplied by a variety of manufacturers. The frequency swing required varies widely. A large frequency swing is required for heavy-ion synchrotrons and a rapid frequency swing is needed for rapid-cycling synchrotrons. Large accelerators have long straight sections with room for many cavities. Other accelerators have little room, few straight sections, or even have stacked rings with small vertical separations, like the PS Booster at CERN. These differences lead to various solutions to the cavity or drift tube design. However, the designs can in general be described by five basic configurations. Finally, designs using materials such as VitroVac, FineMet, and VitroPerm are presented—these achieve broadband behaviour and reduced size compared with ferrite-filled cavities. A comparison between ferrite and VitroVac can be found in Table 2.

2. FERRITE

2.1 Relevant parameters

Naturally occurring ferrous ferrite has the formula Fe_3O_4, often written as $Fe^{3+}(Fe^{2+}Fe^{3+})O^4$ to show the distribution of the metal ions in the crystal structure [2]. A range of ferrites can be produced by replacing the Fe^{2+} ion by any other divalent metal, as long as the ion diameter is comparable to that of the Fe^{2+} ion. Typical divalent metals fulfilling this requirement are nickel, manganese, magnesium, cobalt, copper, zinc, and cadmium.

Ferrite materials with a wide range of magnetic, electrical and mechanical properties can be produced by mixing these different ferrites [2, 3]. The main properties that must be considered for use in RF cavities are magnetic permeability, dielectric constant, resistivity, thermal conductivity, and the effects of temperature and electromagnetic fields on these properties.

Table 1: Parameters of some synchrotrons that use ferrite-tuned cavities

Synchro-tron	No. of cavs.	No. of gaps per cavity	Tuning range (MHz)	Accel-erating time (s)	Max. df/dt (MHz/s)	Gap capacity (pF)	Ind. range (μH)	Type of ferrite	B_{max} in Ferrite (mT)	Bias current range (A)	Tuning system bandwidth (kHz)
ISIS	6	2	1.3–3.1	0.01	325	2200	6.8–1.3	Philips 4M2	10	200–2300	6
CERN PS	11	2	2.8–9.6	0.7				Philips 4L2		3100	
CERN PSB before 1998	1 / ring	1	3–8.4	0.45		80		Philips 4L2		60–800	15
CERN PSB_C02		1	0.6–1.8					Philips 4A11	12		
CERN PSB_C04			1.2–3.9					Philips 4L2	9.4		
CERN PSB_C16			6.0–17.0					Philips 4M2	3.2		
CERN LEAR	2	1	0.38–3.5	0.10		500–3000		Philips 8C12 / Toshiba PE17			
DESY-III	1	2	3.27–10.33	3.6						160–2000	
SACLAY MIMAS	2	1	0.15–2.5	0.2	14			TDK C4 SY7		0–400	
SACLAY SATURNE	2	1	1.7–8.3	0.5				Philips 8C12		-10–200	1–10
COSY	1	1	0.45–1.6	1–3	1.6	1000		Philips 8C12		-10–100	1–10
CELSIUS	1		0.4–2 1–5							1500	
KEK PS	4	2	6–8	0.8	14.5	100	7–4	Toshiba M4B23 μ ~100	7	80–400	3
KEK BOOSTER	2	2	2.2–6	0.025	265	650	8–1	Toshiba M4A23 μ ~150	10	250–2200	1
FNL BOOSTER	18		30.3–52.8	0.033	3000			Stack-pole and Toshiba		50–2250	
BROOKHAVEN AGS	10	4	2.52–4.46	0.6							
BROOK-HAVEN BOOSTER	2	4	2.4–4.2	0.062		395	115–37	Philips 4M2		145–900	
GSI–SIS	2	1	0.85–5.5					Philips 8C12			

The hysteresis loop followed by a ferromagnetic material when subjected to a large field variation is shown in Fig. 3. Added to this is the effect of a smaller, rapidly varying RF magnetic field H_{ac}. As can be seen, the incremental permeability $\mu_r = B_{ac}/(\mu_0 H_{ac})$ varies when the operating point on the hysteresis loop is moved. Thus an inductor made with a ferrite core will have a different value of inductance depending on the magnetic biasing field, and also on the magnitude of the applied H_{ac}. The variation of μ that can be achieved in a particular type of ferrite determines the inductance change that can be obtained. The variation of the incremental permeability with applied field for several grades of ferrite is shown in Fig. 4 [3].

Table 2: Comparison between a ferrite- and a VitroVac-filled cavity

	(h = 1)-cavity	**VitroVac-cavity**
Material	ferrite 8C12, Philips	VitroVac 6025F
Number of toroids	46	24
Frequency range	0.44–2 MHz	0.2– 8 MHz
Tuning current	-20–70 A	0–10 A
Duration of a phase jump	10–50 periods	2 periods
Impedance	ca. 1 kΩ	ca. 300 Ω
RF power	up to 50 kW	10–50 kW
Max. RF amplitude	7100 V peak	2450 V peak
Signal shape	Sinusoidal	Sinusoidal + harmonics

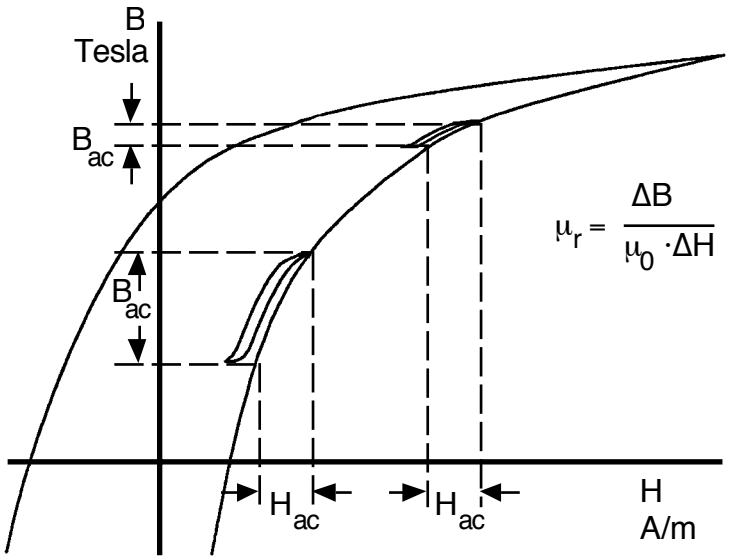

Fig. 3: Ferrite B-H loop with added AC field H_{ac} at two different working points

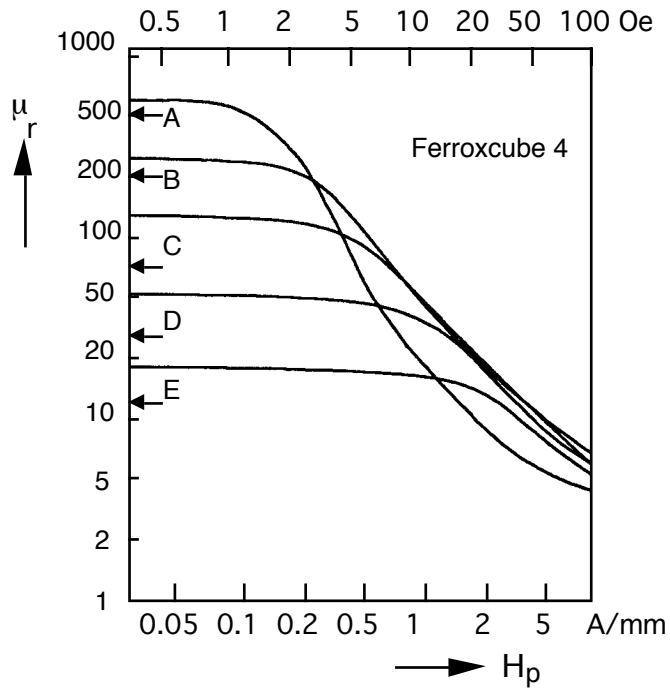

Fig. 4: Plot of μ_r against magnetic bias field H_p for different grades of Philips NiZn ferrite (see also Fig. 6)

2.2 Ferrite inductors

Inductors with ferrite cores offer an increased inductance value compared with an air-cored version, and will also have increased losses due to hysteresis and eddy current loss in the core. The loss can be represented by assigning a complex value to the magnetic permeability:

$$\mu = \mu' - j\mu'' \,. \tag{1}$$

The real part μ' measures the increase in inductance. The imaginary part μ'' is a measure of the core loss. Thus the impedance of the inductor is

$$Z = j\omega\mu L_0 \tag{2}$$

$$= j\omega L_0 \,(\mu' - j\mu'')$$

$$= j\omega\mu' L_0 + \mu''\omega L_0$$

$$= j\omega L + R \,,$$

where L_0 is the value of the air-cored inductor.

$$L = \mu' L_0 \tag{3}$$

$$R = \mu''\omega L_0 \,. \tag{4}$$

The quality of this series circuit is defined as

$$Q = \omega L / R = \omega\mu' L_0 / \omega\mu'' L_0 \tag{5}$$

$$Q = \mu' / \mu'' \,.$$

If this ferrite-loaded inductance is connected across a lossless capacitor, as in Fig. 5, then the impedance of the circuit at resonance can be written as

$$Z = Q\omega L = Q\omega\mu' L_0 \tag{6}$$

$$Z = (\mu' Qf)\, 2\pi L_0 \, .$$

The factor $(\mu' Qf)$ can be regarded as a figure of merit for ferrite materials in a given set-up. Plots of μ' and μ'' against frequency are shown in Fig. 6 for different grades of Philips Ferroxcube 4 [3]. The specifications of the material 8C12 are shown in Fig. 7 [4].

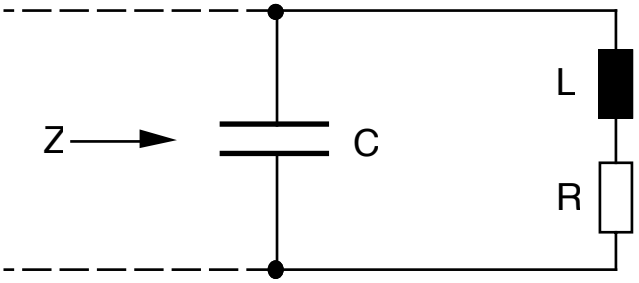

Fig. 5: Parallel resonant circuit with ferrite-cored inductor

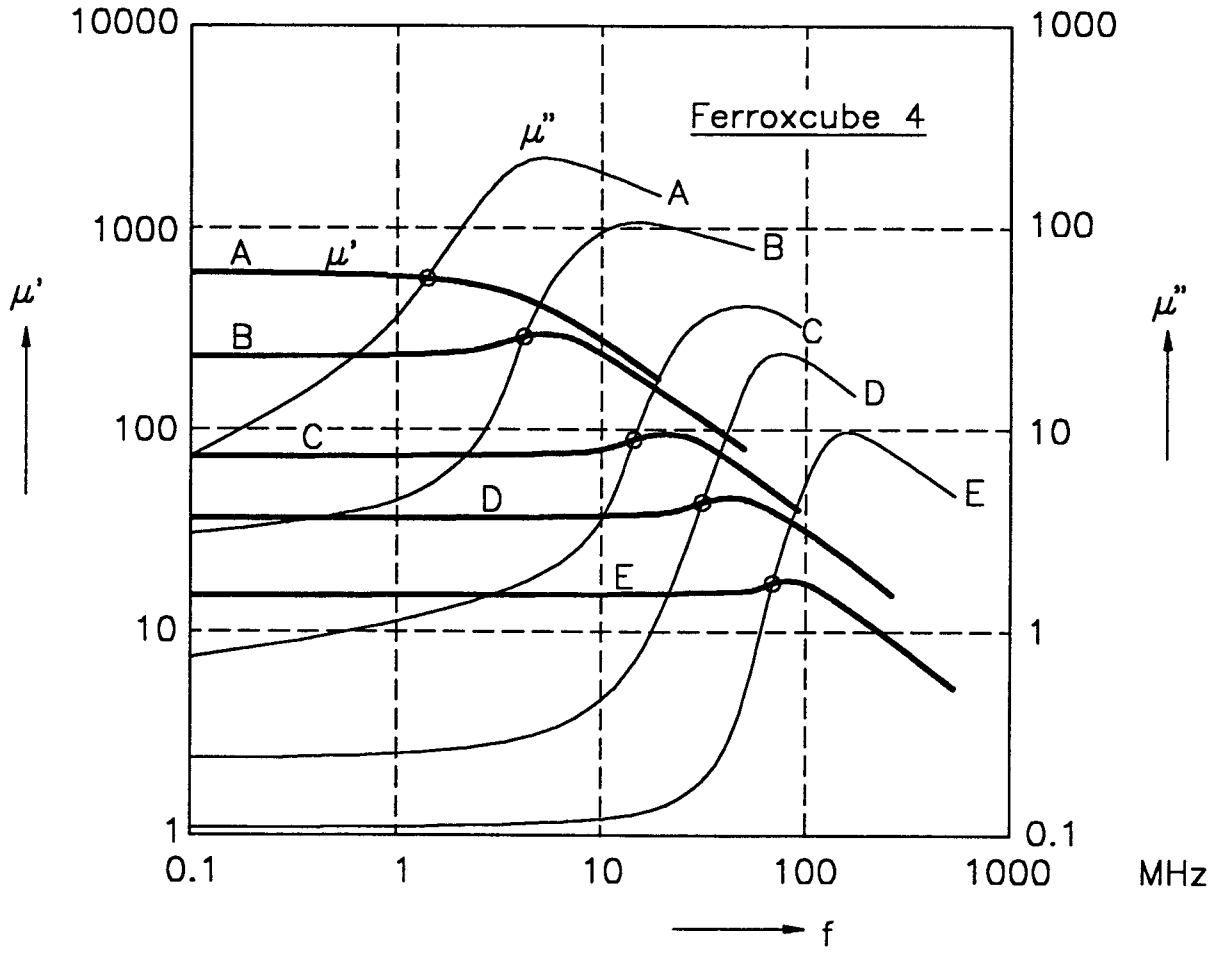

Fig. 6: Plots of μ' and μ'' against frequency for different grades of Philips ferrite

8C12 SPECIFICATIONS

SYMBOL	CONDITIONS	VALUE	UNIT
μ_i	25 °C; ≤10 kHz; 0.1 mT	900 ±20%	
B	25 °C; 10 kHz; 250 A/m 100 °C; 10 kHz; 250 A/m	≈230 ≈150	mT
ρ	DC; 25 °C	$\approx 10^5$	Ωm
T_C		≥125	°C
density		≈5100	kg/m³

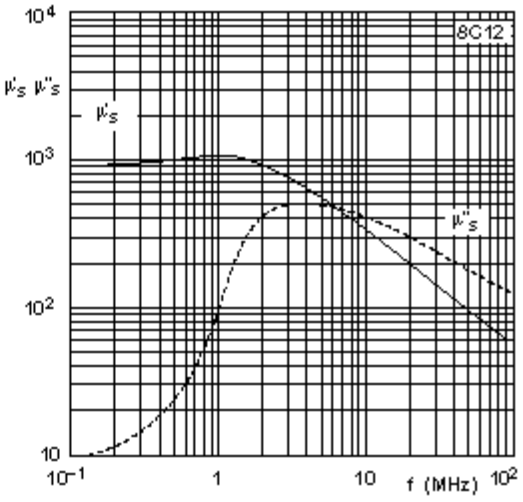

Complex permeability as a function of frequency.

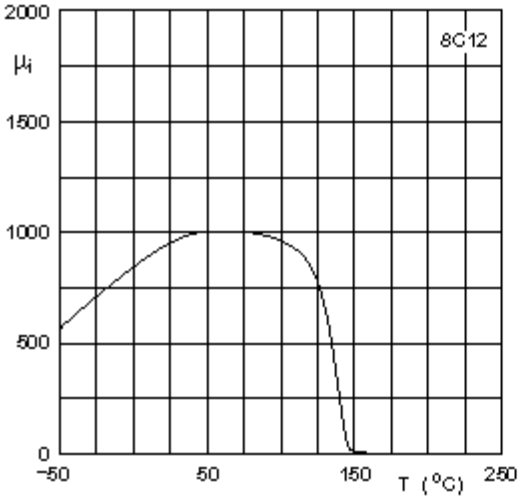

Initial permeability as a function of temperature.

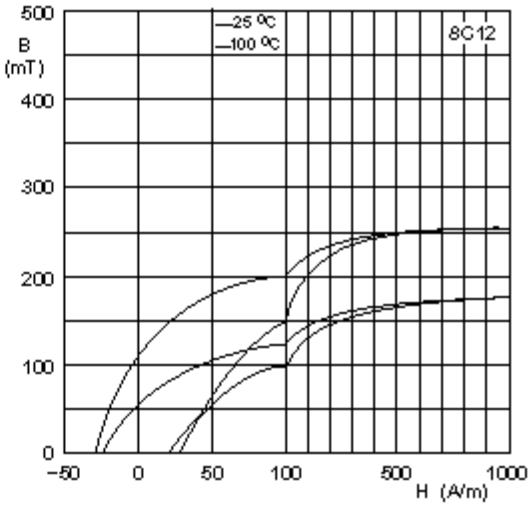

Typical B-H loops.

Fig. 7: Specifications of Philips ferrite 8C12

2.3 Dielectric constant of ferrite

The dielectric loss in ferrite can be treated in the same manner as the magnetic loss by assigning a complex value to the permittivity ε, such that

$$\varepsilon = \varepsilon' - j\varepsilon''. \tag{7}$$

This results in a resistance in parallel with a ferrite filled capacitor:

$$R = 1/\omega\varepsilon'' C_0 \tag{8}$$

where C_0 is the value of the air-filled capacitor. The Q-value obtained when the ferrite-filled capacitor is resonated with a lossless coil is then

$$Q = \varepsilon' / j\varepsilon''. \tag{9}$$

However, with NiZn ferrites, ε' remains constant at a value of about 10 and does not vary with electric or magnetic fields [5]. At frequencies of up to 30 MHz the value of ε'' has not been found to be significant [5]. This is particularly the case with resonators that use metallic cooling plates between the ferrite toroids, when there is very little electric field penetration of the ferrite.

3. COAXIAL RESONATORS

3.1 Characteristic impedance and resonance conditions

Most of the variable frequency RF systems found in accelerators use shorted, ferrite-loaded, coaxial transmission lines as inductors to resonate with the accelerating gap or drift tube capacitance. In the case of the coaxial cavity the beam passes through the hollow central coaxial conductor and is accelerated by the electric field across the end capacitive gap. With the drift tube, the beam is accelerated by the electric fields across the gaps at each end. The drift tube forms a capacitor that is connected to the end of the resonator. The energy gain is dependent on the phase change in these electric fields during the transit time of the beam through the drift tube. In both cases the circuit is tuned to the required accelerating frequency by changing the biasing magnetic field in the ferrite of the resonator. In Fig. 8, C_g represents the gap or drift tube capacitance.

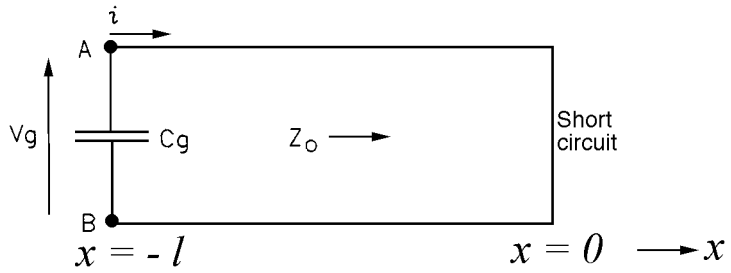

Fig. 8: Basic coaxial resonator circuit as short-circuited transmission line

The reactive part of the impedance of such a resonator at the points AB is

$$Z = j \cdot Z_0 \tan(\omega l / v) \tag{10}$$

where l is the length of the line, v the velocity of the signal in the line, and Z_0 the characteristic impedance of the transmission line.

With $\omega = 2\pi f$ and the wavelength $\lambda = (v / f)$ the relation

$$(\omega l / v) < \pi / 2 \tag{11}$$

is equivalent to

$$(2\pi l / \lambda) < \pi / 2$$

$$\Leftrightarrow 1 / \lambda < 1 / 4 \,. \tag{12}$$

Then Z is inductive

$$Z = j\omega L = j \cdot Z_0 \tan(\omega l / v) \tag{13}$$

with

$$L = (Z_0 / \omega) \tan(\omega l / v) \,. \tag{14}$$

The resonance condition

$$\omega^2 = \frac{1}{LC_g} \tag{15}$$

with the gap capacitor C_g gives the length of the line to reach a desired frequency

$$l = \frac{v}{\omega}\arctan\left(\frac{L\omega}{Z_0}\right) = \frac{v}{\omega}\arctan\left(\frac{1}{Z_0\,\omega C_g}\right) . \tag{16}$$

The inverse function to obtain the frequency has to be solved numerically.

A typical resonator structure is shown in Fig. 9, where the ferrite is in the shape of toroids and each is separated from the next by an air-cooled gap or a water-cooled metal plate. A gap between the inner tube and the cooled metal discs prevents voltage breakdown.

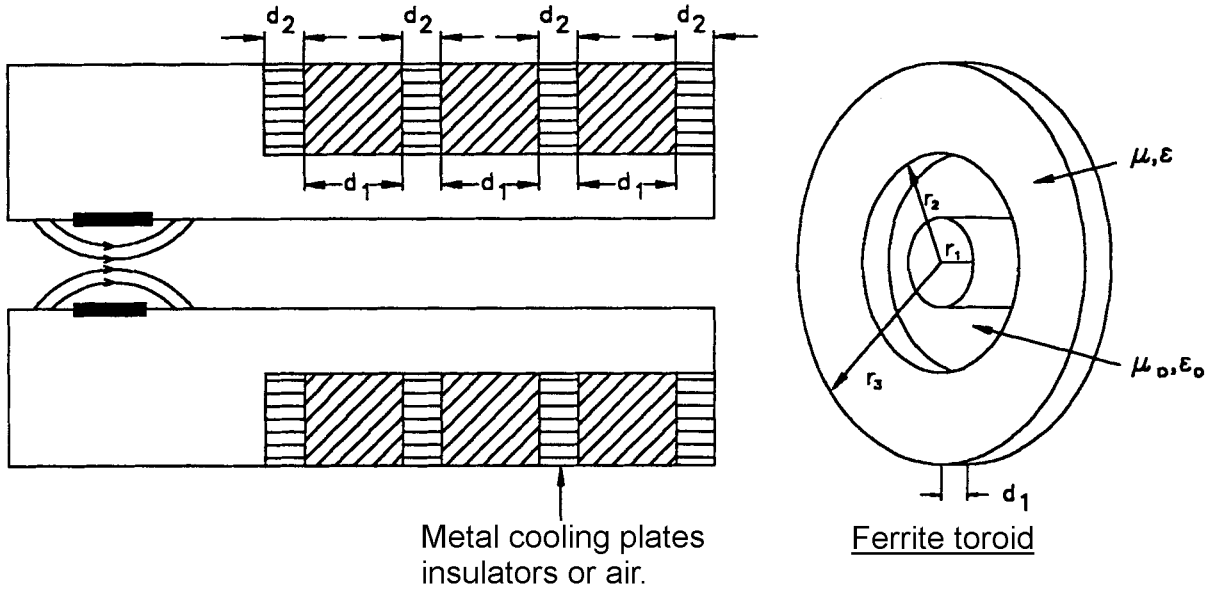

Fig. 9: Typical resonator structure

The capacitance of this line (with the effective ε_e) in farads/metre is

$$C_t = \frac{2\pi\,\varepsilon_e\,\varepsilon_0}{\ln\frac{r_3}{r_1}} \tag{17}$$

and the inductance (with the effective μ_e) in henrys/metre is

$$L_t = \frac{1}{2\pi}\;\mu_e\,\mu_0 \ln\frac{r_3}{r_1} . \tag{18}$$

The effective permittivity ε_e is:

- case 1 for an air-filled gap

$$\varepsilon_e = \frac{\varepsilon}{k + \varepsilon\,(1-k)}\;\frac{d_1}{d_1 + d_2} \tag{19}$$

- case 2 for a resonator with cooled metallic plates

$$\varepsilon_e = \frac{1}{1-k} \tag{20}$$

The effective permeability μ_e is in both cases

$$\mu_e = \left(1 + k\ (\mu' - 1)\right)\ \frac{d_1}{d_1 + d_2} \tag{21}$$

with (derivation in Appendix A)

$$k = \ln\frac{r_3}{r_2}\ \Big/\ \ln\frac{r_3}{r_1}\ . \tag{22}$$

Example: material grade 8C12 used in COSY (h = 1) ferrite cavity:

$r_1 = 0.1$ m, $r_2 = 0.125$ m, $r_3 = 0.25$ m, gives k = 0.76, $\varepsilon_e = 4.1$

$d_1 = 25$ mm, $d_2 = 6$mm, $\mu' = 700$, gives $\mu_e = 427$ (e.g. 60%).

The wave velocity (with c_0 = velocity of light) in such a line is

$$v = \frac{1}{\sqrt{L_t\, C_t}} = \frac{c_0}{\sqrt{\mu_e\, \varepsilon_e}}\ . \tag{23}$$

The characteristic impedance of this loaded line is

$$Z_0 = \sqrt{\frac{L_t}{C_t}} = \frac{1}{2\pi}\ \ln\frac{r_3}{r_1}\sqrt{\frac{\mu_e\, \mu_0}{\varepsilon_e\, \varepsilon_0}}\ = 60\ \Omega\ \ln\frac{r_3}{r_1}\ \sqrt{\frac{\mu_e}{\varepsilon_e}}\ . \tag{24}$$

If the voltage at the capacitor is given as a complex vector $V_g(t) = V_g\, e^{j\omega t}$, the voltage *V(t, x)* and current *i(t, x)* are given by

$$V(t,x) = -V_g\ \ e^{j\omega t}\ \frac{\sin\dfrac{\omega\, x}{v}}{\sin\dfrac{\omega\, l}{v}}\ , \tag{25}$$

$$i(t,x) = jV_g\ \ e^{j\omega t}\ \frac{\cos\dfrac{\omega\, x}{v}}{Z_0\ \sin\dfrac{\omega\, l}{v}} \tag{26}$$

(derivation in Appendix B).

The current is at a maximum at the short circuit where $x = 0$ and the ratio of the current at $(x = -l)$ to the current at $(x = 0)$ is

$$\frac{i(x = -l)}{i(x = 0)}\ = \frac{\cos\dfrac{\omega\ l}{v}}{1} = \cos\frac{\omega\ l}{v}\ . \tag{27}$$

This ratio determines the difference in the RF magnetic fields in the toroids at both ends of the resonator. Resonators are usually designed to keep this difference within about 10%, indicating a value of $(\omega l / v) <$ arc cos (0.9) = 26°.

3.2 RF magnetic induction in the ferrite

In Fig. 10 the magnetic field H at radius r and the induction B due to the current i are

$$H(r) = \frac{i}{2\pi r} \qquad B(r) = \mu\mu_0 \frac{i}{2\pi r} . \tag{28}$$

The maximum induction B_{rfmax} is at the radius $r = r_2$ and longitudinal at the short circuit where i is a maximum in the resonator (I is the current at $x = -l$):

$$B_{rf\ \max} = \mu\mu_0 \frac{I}{2\pi r \cos\dfrac{\omega l}{v}} . \tag{29}$$

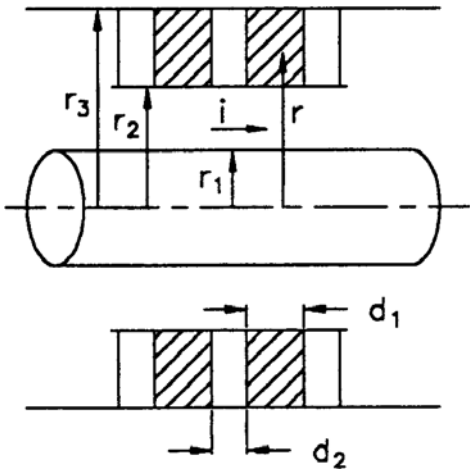

Fig. 10: Magnetic induction in the ferrite at radius r

In NiZn ferrites, where the saturation field is 0.2–0.3 T, the maximum value of B_{rf} is usually kept below 0.01 T. The Q-value of the ferrite will decrease as B_{rf} is increased. A typical graph of $(\mu' Qf)$ against B_{rf} is shown in Fig. 11. [6]

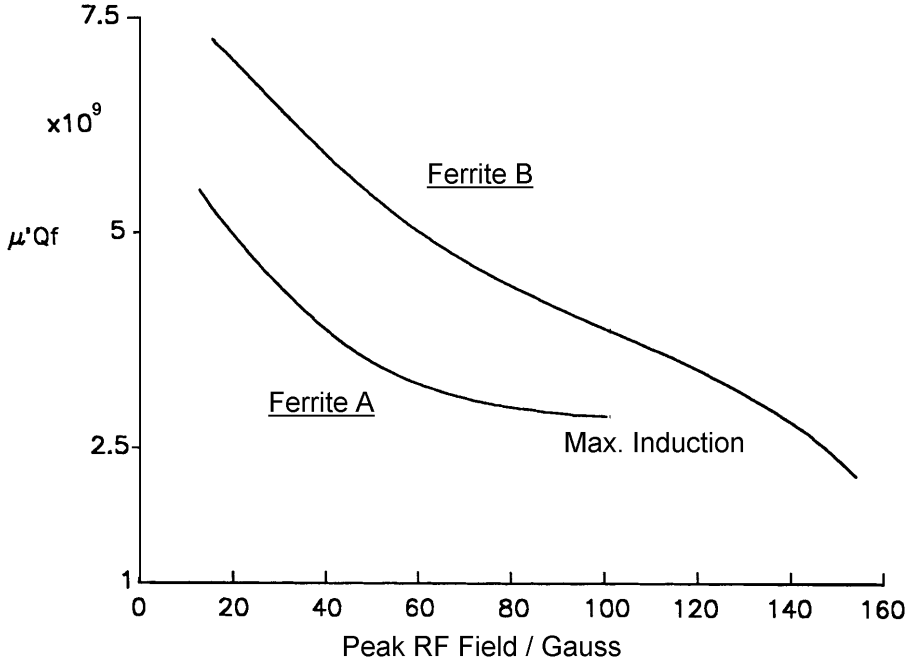

Fig. 11: Plot of $(\mu' Qf)$ against peak RF field at 2.0 MHz

The required resonator length (derivation in Appendix C) for a given cap voltage V_g is estimated from

$$l = \frac{V_g \ \mu}{\mu_e \, r_2 \ln \frac{r_3}{r_1} \ \omega \ B_{rf\,\max}} \ . \tag{30}$$

3.3 Power dissipation in the ferrite

The equivalent circuit of the resonator in Fig. 12 describes losses with $R = Q\omega L$.

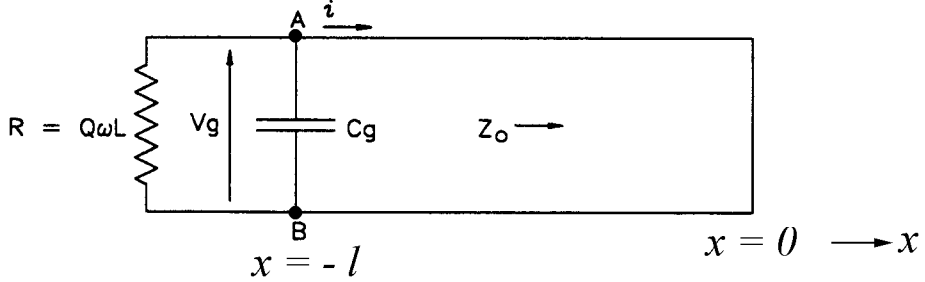

Fig. 12: Diagram of transmission line with C_g and resistor R.

The power dissipation in the resonator is

$$P = \frac{V_g^2}{2R} = \frac{V_g^2}{2Q\omega L} \ , \tag{31}$$

where P is the total power in the resonator, and V_g the peak RF voltage (amplitude) on the end of the resonator. The mean power per unit length in the resonator is

$$P_{mean} = \frac{V_g^2}{2lQ\omega L} \ \text{[W/m]} \ , \tag{32}$$

where Q will vary with voltage and frequency. The power dissipation along the resonator, $P(x)$, depends on the square of the current, i^2.

$$P(x) = P_{\max} \cos^2 \frac{\omega x}{v} \ \text{[W/m]} \tag{33}$$

$$P_{mean} = \frac{P_{\max}}{2} \left(1 + \frac{\sin \frac{2\omega l}{v}}{\frac{2\omega l}{v}} \right) \ \text{[W/m]} \ . \tag{34}$$

The maximum power density in a ferrite toroid and the temperature rise T is given by

$$P_{d\,\max} = P_{\max} \frac{d_1 + d_2}{\pi \left(r_3^2 - r_2^2 \right) d_1} \ \text{[W/m}^3\text{]} \tag{35}$$

$$T = \frac{P_d}{k} \ \frac{d_1^2}{4} \ \text{[degrees]} \ , \tag{36}$$

where k is the thermal conductivity of the ferrite in (W/mK), and P_d the power density in the ferrite in (W/m^3).

With thermal conductivities of k = (3.5 W / mK) and a toroid thickness of 25 mm the power density is limited to 100–300 W/l for most NiZn ferrites. The usable power density depends on ferrite properties and mechanical design. A rise in the ferrite temperature increases the μ-value and decreases the Q-value [5]. Finally, the μ-value decreases rapidly as the Curie temperature of the ferrite is reached. This can lead to thermal runaway in the ferrite.

3.4 High loss effect

High loss effect is exhibited as a time-dependent phenomenon, and it occurs when the stored energy in ferrite is raised above a threshold level of (3 ± 1) x 10^{-7} J/cm^3 [7]. At this power density the Q of the resonator drops after a period of time and the voltage across the resonator becomes unstable.

4. THE EFFECT OF MAGNETIC BIAS FIELDS ON FERRITE

4.1 The comparison of parallel and perpendicular magnetic bias fields

The application of a magnetic field to ferrite leads to a change in the incremental permeability, and this field can be applied either parallel or perpendicular to the RF field. As most of the systems in use today use parallel bias this will be discussed first. Plots of the incremental permeability, μ, as a function of the magnetic biasing field were shown for five grades of ferrite in Fig. 4. In general the ferrites with high values of initial permeability will change the permeability at lower values of applied bias field. The frequency range over which the system can be tuned is given by the change in μ' value.

$$\omega^2 = \frac{1}{LC_g} \qquad \omega \tan\left(\frac{\omega l}{v}\right) = \frac{1}{Z_0\ C_g} \tag{37}$$

Relations to the permeability μ':

$$v \propto \frac{1}{\sqrt{\mu'}} \qquad \omega \propto \frac{1}{\sqrt{\mu'}} \qquad Z_0 \propto \sqrt{\mu'}\ . \tag{38}$$

So the ratio of maximum to minimum frequency is given by $\sqrt{\frac{\mu_{\max}}{\mu_{\min}}}$, (39)

where $\mu_{\max}$ is the maximum value of μ' at the minimum bias field, and $\mu_{\min}$ is the minimum value of μ' at the maximum bias field.

It has been demonstrated [5, 8, 9] that the use of a bias field perpendicular to the RF field significantly reduces losses in the ferrite. It has also been found that the change in μ for a given value of perpendicular bias field is much reduced compared with that for a parallel bias field. This lower loss is explained by the fact that the ferrite is operated closer to magnetic saturation. There is great interest in this type of biasing for resonators working at the higher frequency end of the spectrum (around 50–80 MHz) [8].

4.2 Dynamic loss

Dynamic loss in a resonator is observed as a decrease in Q of the resonator subject to changing bias field as compared with that of a resonator with a fixed bias field [7]. This loss is not associated with the bandwidth of the resonator but is very dependent on the ferrite mixture used. It is therefore important to measure ferrite performance at the rate of change of bias field at which it will be used.

5. COMMON DESIGNS AND THEIR EQUIVALENT CIRCUITS

5.1 General considerations

Accelerating structures can be divided into two main types, depending on whether the system uses drift tubes plus coaxial resonators or coaxial cavities. A third type, which needs to tune over only a small frequency range, uses a coaxial cavity with a loosely coupled external resonator. Most other variations are introduced by the necessity of providing a variable bias field to change the ferrite μ' value. A further division can be made between those that apply the bias field in parallel with the RF field and those that apply it perpendicularly to the RF field.

A typical synchrotron RF system is shown in Fig. 13. The cavity is kept in tune with the frequency required for acceleration by the servo control of the cavity bias field current. When in tune, the cavity presents a purely resistive load to the tetrode. To achieve this, the servo keeps the cavity voltage in antiphase to the grid voltage of the tetrode. The bias field current may swing from a few amps to a few thousand amps while covering the frequency range of the RF [10].

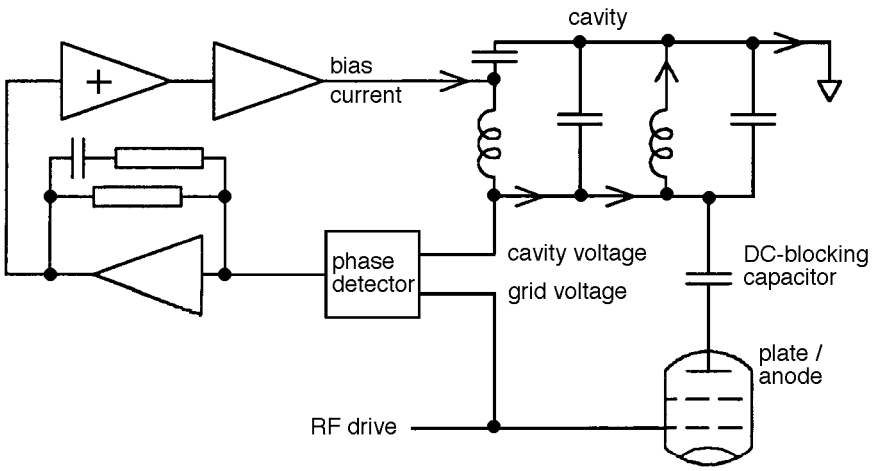

Fig. 13: Servo control of cavity tuning

5.2 Type 1 cavity

Figure 14 shows the main elements of an ISIS cavity. It is very similar to the design of a CERN PS cavity. The water-cooled plates, which provide the ferrite cooling, can be seen separating the 35 ferrite rings in each resonator. The centre tube of the co-ax is made from two coaxial tubes. The outer tube is made from copper to provide low impedance for the bias field current and the RF. The inner tube is made from nickel-plated mild steel to provide the vacuum pipe and to shield the beam aperture from any magnetic field produced on the beam axis by the bias field. The two accelerating gaps are ceramic, metallized at the ends and welded to the mild steel.

The simplest equivalent circuit is shown in Fig. 15. The total capacitance at a gap is represented by C_g, and includes the cap capacitance, the added capacitance, and the stray capacitance. The two gaps are connected in parallel by two 70 Ω coaxial lines that carry both the bias field current and the RF voltage. The RF by-pass capacitor, C_b, forms a low impedance for the circulating RF current in one of the resonators but allows the bias field current to be fed around both resonators, which are in series with the bias current. The bias field is parallel to the RF field but in the opposite direction in each resonator. With a gap voltage of 14 kV, peak C_b must be about 10,000 C_g to limit the RF voltage appearing across the bias field supply to less than a few volts.

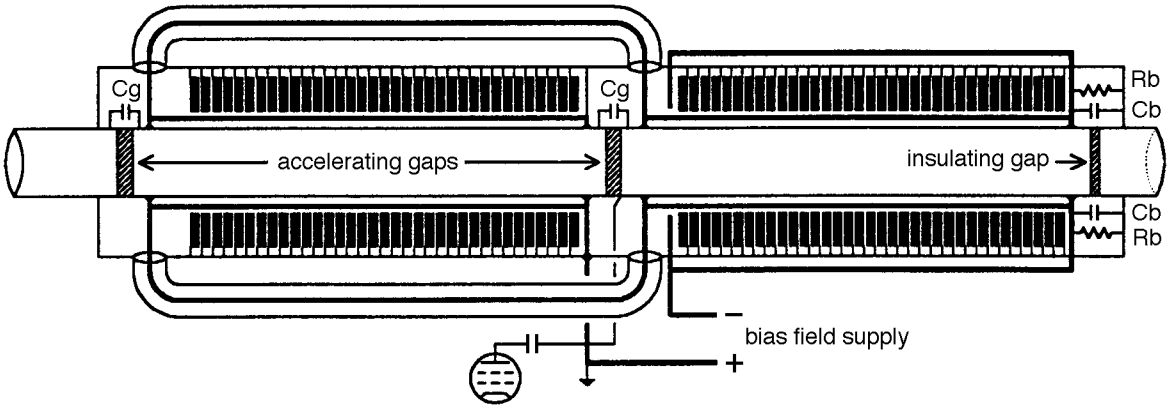

Fig. 14: Type 1 cavity (ISIS)

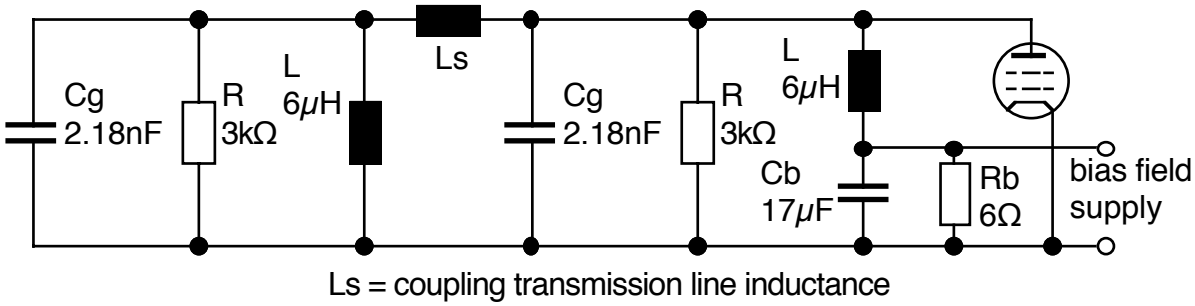

Fig. 15: Type 1 cavity (ISIS) equivalent circuit

The load presented to the RF amplifier is that of the two cavities in parallel. The bandwidth of this circuit is just $f_0/(2Q)$ and the minimum value for this on ISIS is 6.5 kHz in the swept condition. The capacitor C_b and the two resonators also form a tuned LC load for the bias field system. The resonance frequency is

$$f = \frac{1}{2\pi\sqrt{2LC_b}} \quad . \tag{40}$$

In ISIS this frequency has a minimum value of 10.4 kHz. Thus any control loop on the bias supply involving phase modulation of the cavity voltage will incorporate two bandwidth limiting time constants. In ISIS the Q of the resonance produced by C_b is reduced to near unity by a 6 Ω resistor in parallel with C_b. The time constant associated with C_b will decrease as L reduces. The time constant associated with the cavity Q will vary with frequency and gap voltage, and will also depend on whether the cavity is sweeping or not. If stable operation in all conditions is required then the worst-case bandwidths must be catered for. These limiting bandwidths should be taken into consideration in the design of the RF system. An approximation of the phase error in the cavity tuning caused by bandwidth limitations is given by the response to a ramped frequency input.

Phase error

$$\Phi_e = K\left[t + \tau\left(e^{-t/\tau} - 1\right)\right] \tag{41}$$

and Φ_e steady state will be

$$\Phi_e = K\tau \quad , \tag{42}$$

where $1/(2\pi\tau)$ is the tuning system bandwidth, and Φ_e the cavity voltage phase error.

The constant K describes the relation to the acceleration ramp

$$K = \frac{df}{dt}\ \frac{\pi Q}{2 f_0}\ . \tag{43}$$

There (df/dt) is the maximum rate of chance of RF frequency, and f_0 the frequency at which (df/dt) is a maximum.

5.3 Type 2 cavity

Figure 16 shows the main elements of an FNL Booster Synchrotron RF drift tube accelerating system. Each resonator consists of two resonators joined in parallel at the high-voltage end. The bias field is parallel to the RF field and is in the same direction through each resonator half. The RF currents are in opposite directions in each half. The RF voltage induced in a bias winding is zero. There are three resonators in parallel around the drift tube (only one is shown here). The three parallel resonators reduce the minimum inductance value at high bias field to a lower value than could be achieved with a single resonator. The series inductance is minimized between the resonators and the drift tube, and the power tetrode anode and the drift tube. The resonators each have 10 turns for the bias field windings.

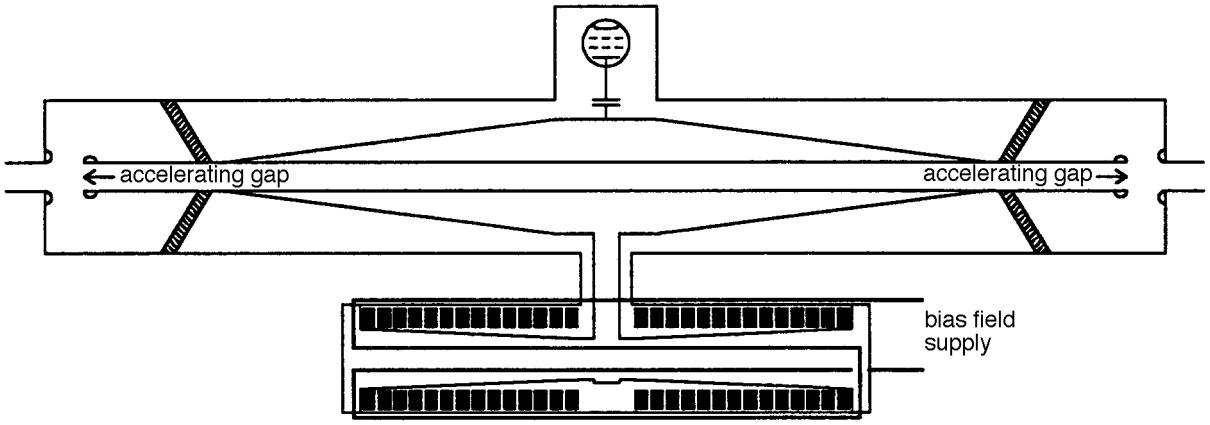

Fig. 16: FNL Booster drift tube system

The equivalent circuit in Fig. 17 is similar to that of the Type 1 system, if a single-turn bias field winding is used. No RF bypass capacitor is used. The inner conductor of the resonator is resistive and the turn formed by the inner and outer resonator conductors is driven by the bias field supply. For multiple-turn bias field windings the induced current is proportionally reduced. The bandwidth limit set by the cavity load for the tuning system is determined only by $f_0/(2Q)$.

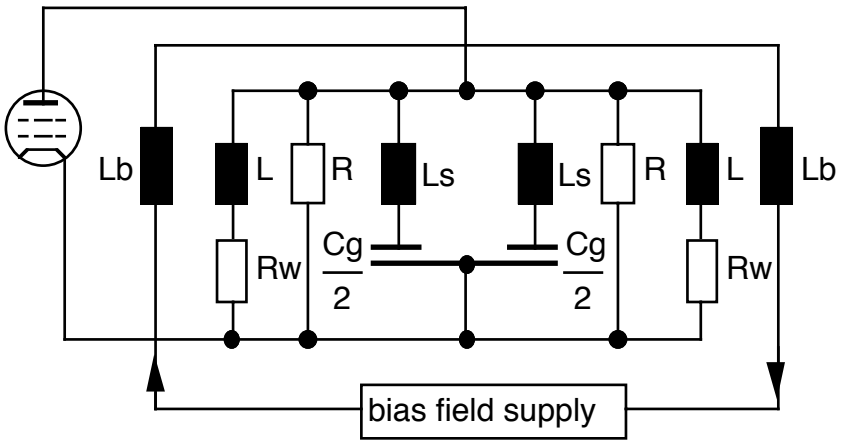

C_g = drift tube Capacity

R_w = wall resistance inside co-ax in resonator

R = ferrite loss in resonator

L_b = bias winding inductance

L = inductance of resonator

L_s = series inductance to drift tube end

Fig. 17: Drift tube system equivalent circuit

5.4 Type 3 cavity (PS Booster, COSY, SATURNE)

In this type of cavity (Fig. 18), which is typified by the former CERN PS Booster cavity, a virtual RF ground exists in the middle of the accelerating gap and the voltages on the resonators are in anti-phase. The bias field is parallel to the RF field but in opposite directions in each half of the cavity. The RF currents are in the same direction in each half of the cavity. The RF amplifier can have a single-ended or differential output, as there is strong coupling between the two cavities via the bias field winding. The bias field windings are arranged as a figure of eight to produce balanced RF voltages on each winding and no RF voltage on the ferrite bias source. The equivalent circuit is shown in Fig. 19 with the circuit as seen by the bias supply in Fig. 20. More information about the status of the CERN Booster cavities operating at different harmonics can be found in Ref. [11]. A view of the installation of the ferrite cavity of COSY is given in Fig. 21. Figure 22 shows the arrangement of ferrites, tuning loop, and cooling discs near the acceleration gap.

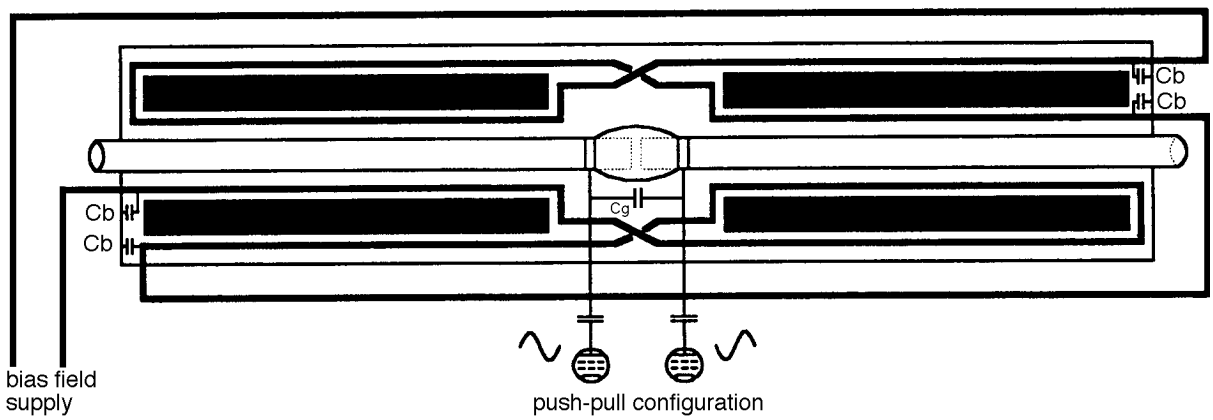

Fig. 18: CERN PS Booster/COSY/SATURNE cavity

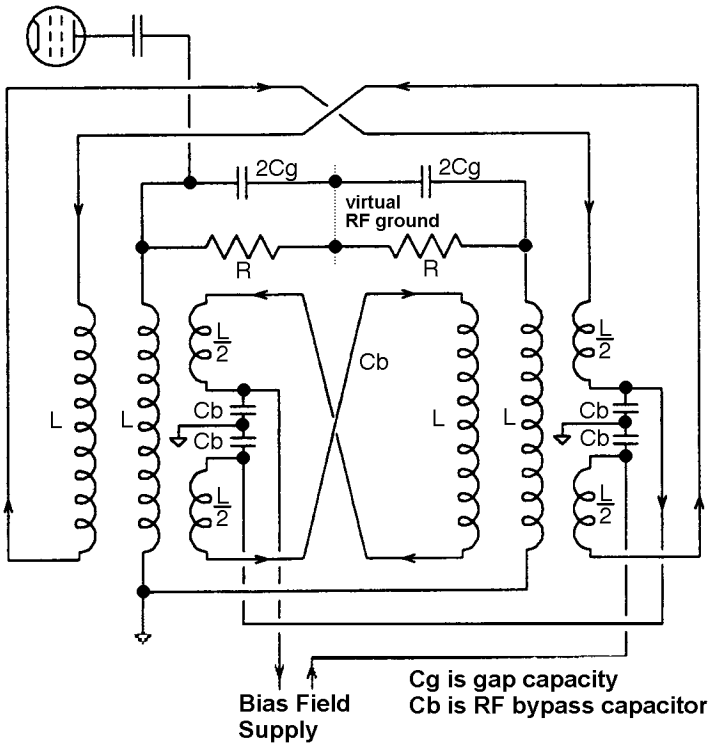

Fig. 19: CERN PS Booster cavity equivalent circuit

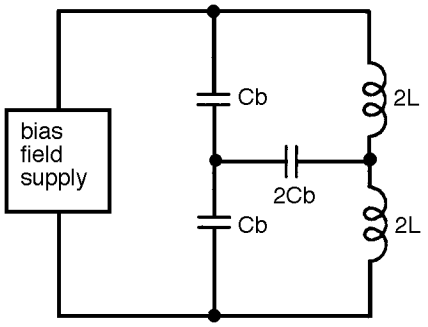

Fig. 20: CERN PS Booster equivalent load for bias field supply

The bandwidth limits set by the cavity on the bias field tuning system are as for Type 1, $f_0 / (2Q)$ and

$$f = \frac{1}{2\pi\sqrt{2LC_b}} \qquad K = \frac{df}{dt}\,\frac{\pi}{2}\,\frac{Q}{f_0} \qquad \Phi_e = K\tau \ . \tag{44}$$

Example for a COSY cavity, shown in Figs. 21 and 22:

(df / dt) = 1.6 kHz / ms at f_0 = 655 kHz,

Q = 10, τ = 1ms gives **K = 0.038 / ms, Φ_e = 2.2°**

As RF voltage is carried by the bias field, winding care must be taken to avoid voltage breakdown from the bias conductors and to avoid RF resonances involving the bias conductors. This becomes increasingly difficult with higher numbers of turns.

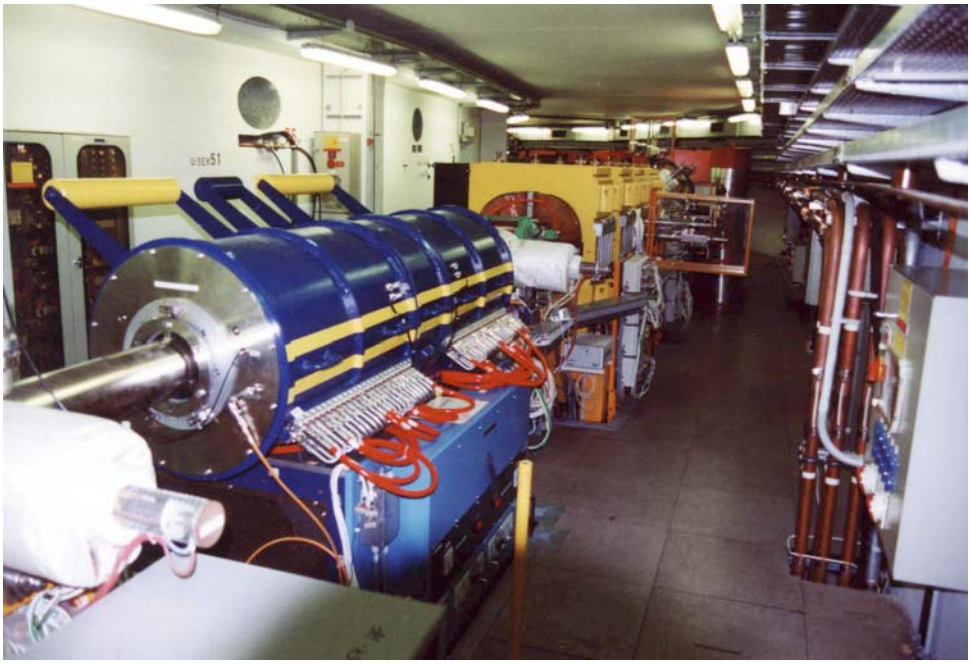

Fig. 21: (h = 1) ferrite cavity of COSY

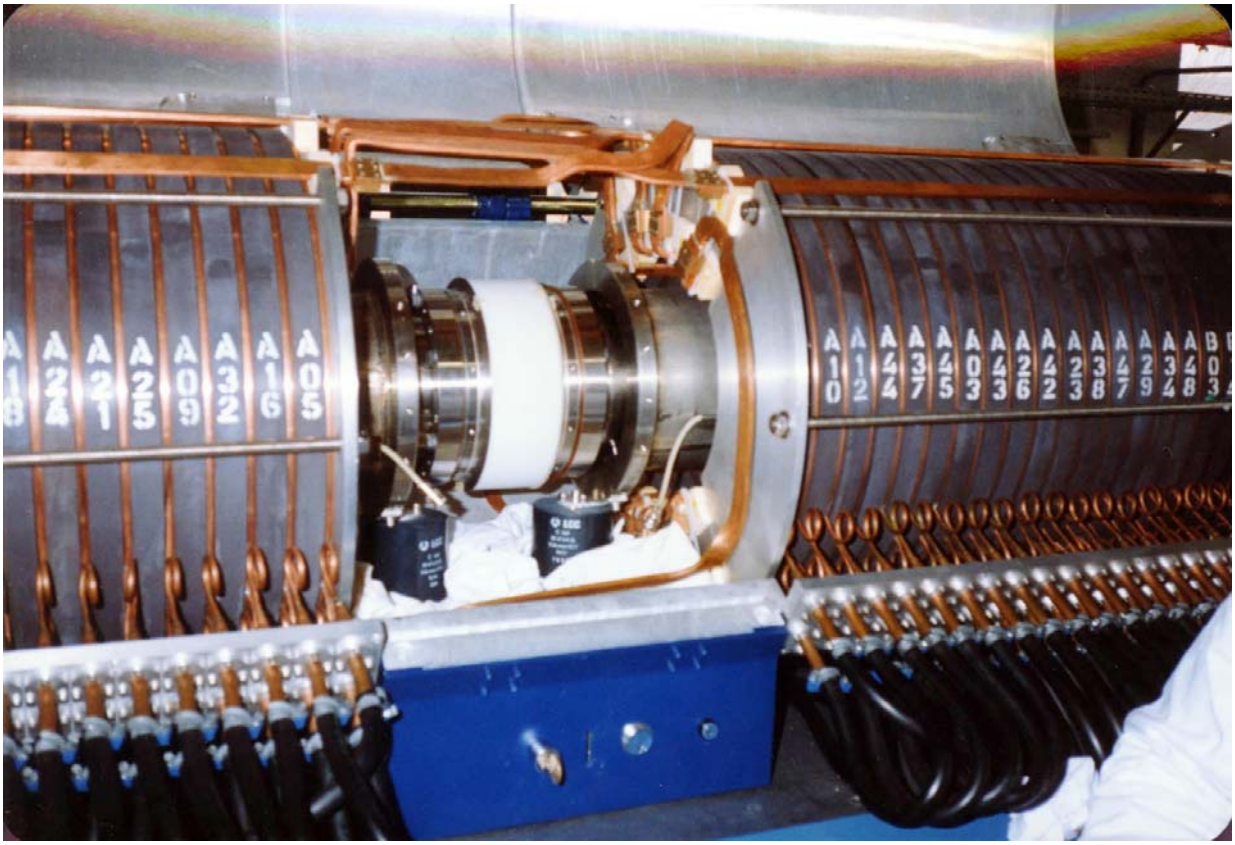

Fig. 22: Arrangement of gap, 8C12 ferrites, and cooling plates in COSY (h = 1) cavity

5.5 Type 4 cavity

This type of cavity (CERN LEAR-type), shown in Fig. 23, is asymmetric and uses a single gap. With this arrangement of bias winding, the induced RF voltage on the winding is constrained to be zero at the bias field supply feed point by splitting the winding at the mid-voltage point on the cavity. The two windings are then crossed in a figure-of-eight mode as in Type 3. In the equivalent circuit (shown in Fig. 24), the parallel bias produces a field that changes direction at the crossover point of the bias winding.

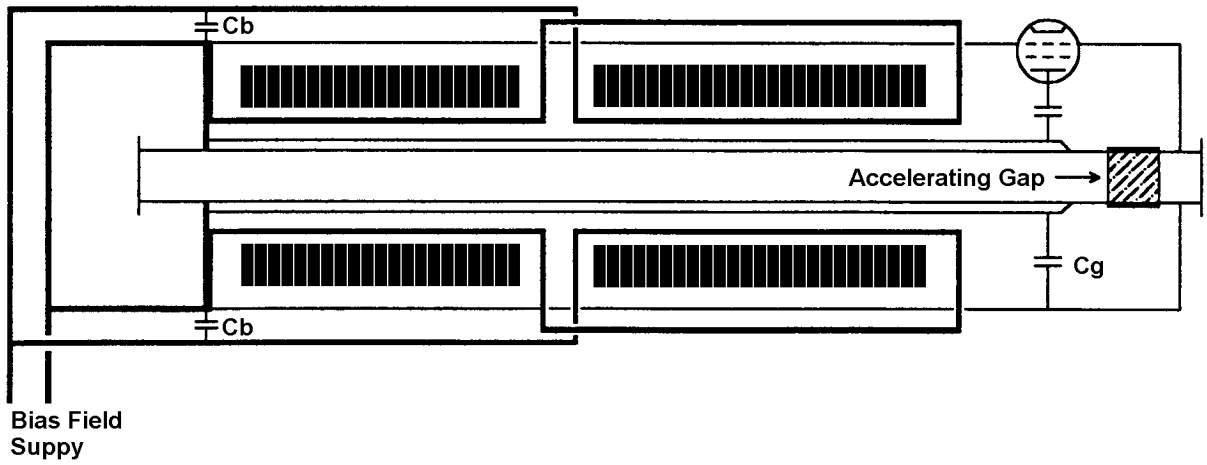

Fig. 23: CERN LEAR-type cavity

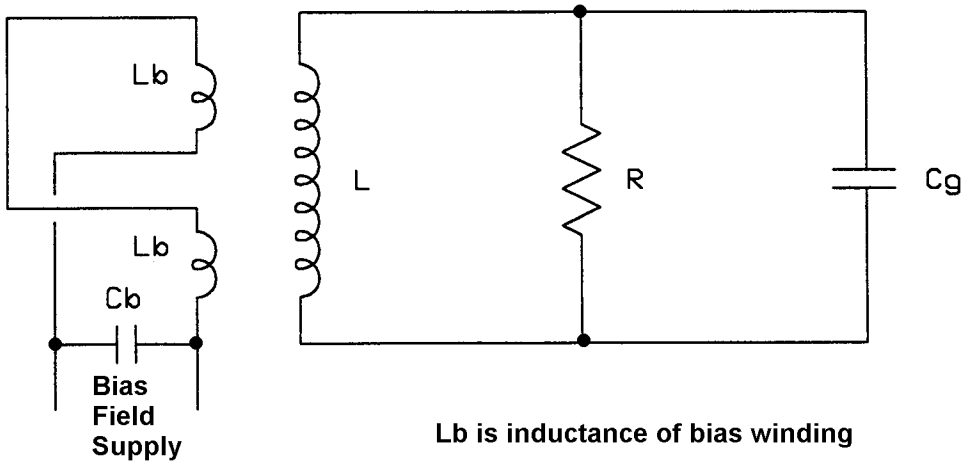

Fig. 24: CERN LEAR-type equivalent circuit

5.6 Type 5 cavity

In this cavity another solution for the single-gap cavity is obtained by using a perpendicular bias field on the ferrite. This is the Los Alamos/TRIUMF type of cavity (Fig. 25). Perpendicular bias and the use of microwave ferrite resulted in a compact cavity with high Q in the 46–61 MHz frequency range. The high Q allows a higher gap voltage and reduces the number of cavities required in the accelerator. The power tube is capacitively coupled to the cavity, whereas the coupling in Types 1 to 4 is a combination of inductive and capacitive coupling.

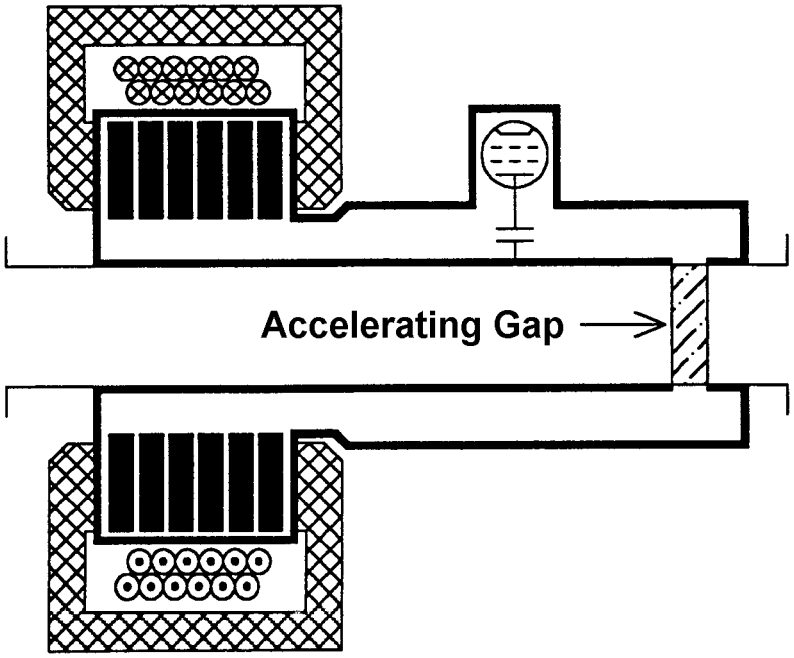

Fig. 25: Los Alamos/TRIUMF cavity

The ferrite is located at the short circuit end of the cavity and the bias field is applied by a solenoidal winding. The cavity outer conductor and short circuit require cuts to reduce the eddy current heating caused when the bias field is changed. The eddy current load is supplied by the bias field supply. This arrangement precludes the use of metallic cooling plates between the ferrite toroids. Furthermore, because a perpendicular bias field is used with low values of μ, then a high value of bias field must be supplied, and this results in some stray field on the beam axis. Figure 26 shows the equivalent circuit. Another possible way of creating a perpendicular field involves the use of a quadrupolar field. An example of this [9] is shown in Fig. 27, a cavity built at the Indiana University Cyclotron Facility. The principle of such a cavity was first demonstrated in 1989 at MPI, Heidelberg.

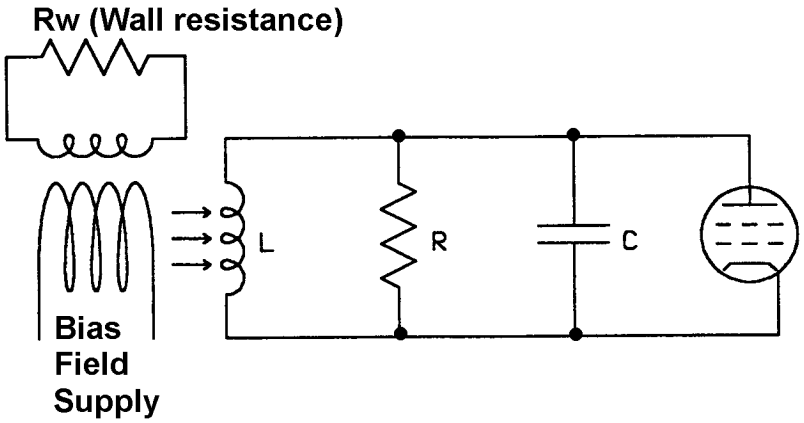

Fig. 26: Los Alamos/TRIUMF cavity equivalent circuit

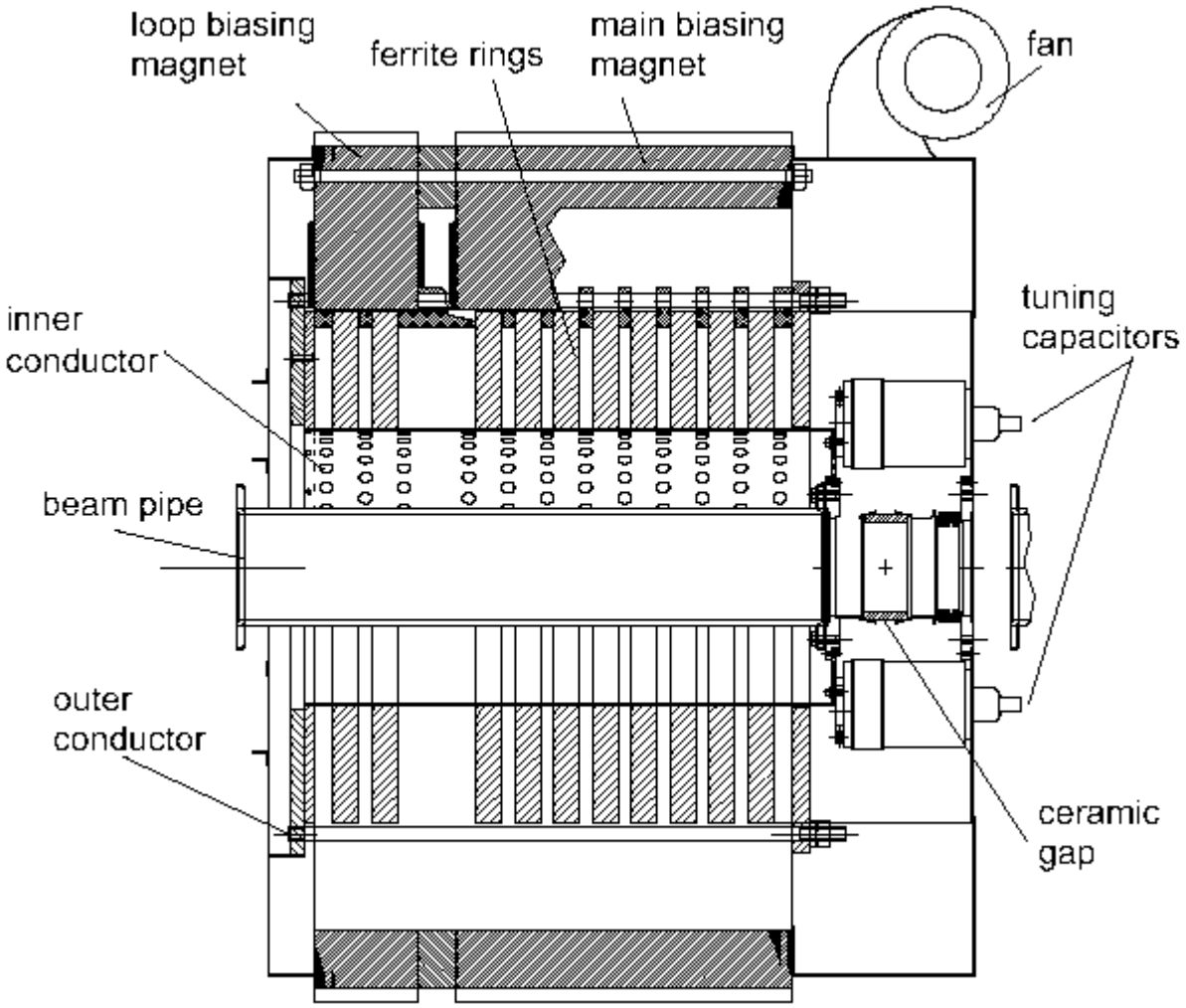

Fig. 27: RF cavity of CIS, Bloomington, Indiana, tuned with a quadrupole field

6. HIGH-ORDER MODES

Unwanted high-order modes in ferrite cavities are only briefly mentioned here. The first resonant mode above the fundamental mode will occur at such a frequency that the resonator appears to be 180° long. As resonators are, in general, designed to be less than 26° long in order to maintain a low variation in B_{RF} in the ferrite, then the next mode is likely to be more than five times the frequency of the fundamental. Additional resonant modes are likely to be caused by multi-turn bias field windings and coaxial coupling arms.

7. BROADBAND CAVITIES

Traditionally, radio-frequency accelerating structures in accelerator rings are made from one or more cavities. Consequently, these structures can transmit only narrow-band frequency signals to the particle beam. While such narrow-band structures require dynamic tuning during the acceleration cycle of a synchrotron, they limit noise transfer to the particle beam to a narrow frequency regime. Moreover, the generation and amplification of harmonic RF signals is a standard procedure, and resonant cavities offer considerable efficiency with respect to power utilization. These are some of the reasons why resonant cavity structures have been used throughout and are used (with very few exceptions) as accelerating structures in accelerators.

Increasing demands on specific accelerating voltage waveforms have led to the installation of more complex accelerating systems, whether they use a set of cavities to run at harmonics [11, 12], or a broadband electrostatic structure [13].

Such specific demands on accelerating voltage waveforms of more than one frequency component, or even strictly non-harmonic waveforms, such as the saw-tooth type, may stem from the need to tailor particle bunch shapes or dynamics, e.g. for the passage of points of instability, or the synchronized transfer to another accelerator [12–14].

In addition to the accelerating structure and the associated power amplifiers, the low-level signal generation and dynamic control has to comply with these specific voltage waveform demands. Because of the broadband feature, signal generators must have unprecedented purity or lack of spurious frequency emissions at high frequency variability.

At CRYRING, a small ring for many different ion species, experiments were performed with a double-gap drift-tube structure without material [15]. A simplified layout is shown in Fig. 28. After the particles cross the first gap, they fly through a drift tube and then cross the second gap. The particles gain an amount of energy determined by the voltage on the central drift tube and the change of the signal during the flight through the drift tube. This structure is broadband (10 kHz to 1.5 MHz) without tuning, so one can apply a waveform that is a repeated sequence of parabolas (Fig. 29), and the particles will experience an energy gain, as if they had seen a saw-tooth signal at a single gap.

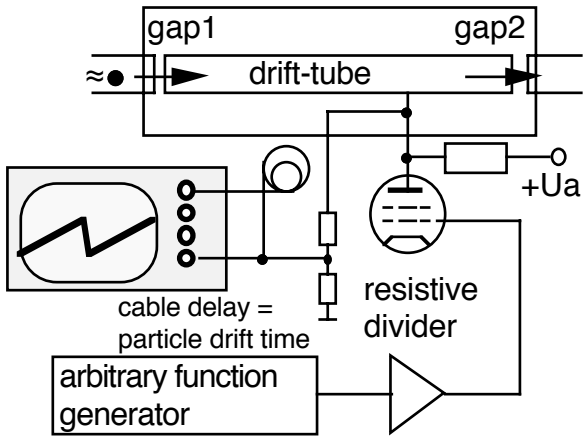

Fig. 28: Drift tube structure at CRYRING

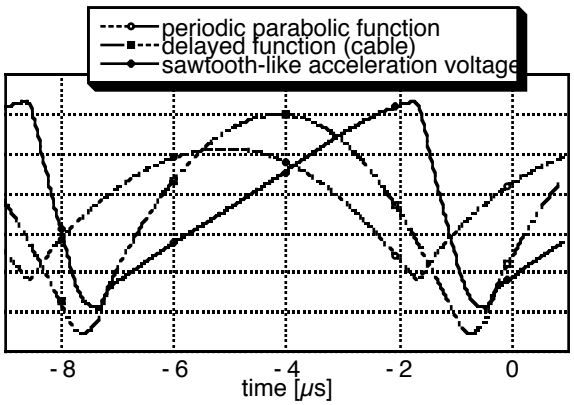

Fig. 29: Application of a parabolic waveform

Another approach to broadband operation is to apply a load resistor in parallel to the gap of a ferrite cavity [16]. This reduces the external quality of the resonator, so one therefore has to balance power efficiency with broadband behaviour.

7.1 VitroVac cavity

Instead of ferrite, one can use amorphous magnetic materials that are wound like magnetic tapes to obtain a toroid shape. A cavity with VitroVac 6025F was constructed at SATURNE for MIMAS as proof-of-principle [17]. A cut-away drawing of this cavity is shown in Fig. 30 and the system layout is described in Fig. 31. The hysteresis curve of the material 6025F is displayed in Fig. 32.

This cavity still needs tuning, but the current is lower compared to a ferrite-filled cavity. The impedance as a function of the tuning current is displayed in Fig. 33. Such a cavity allows almost arbitrary waveforms if enough RF power is available for the higher harmonics, which have to be adjusted in amplitude and phase, is available. Examples are shown in Figs. 34(a) and 34(b).

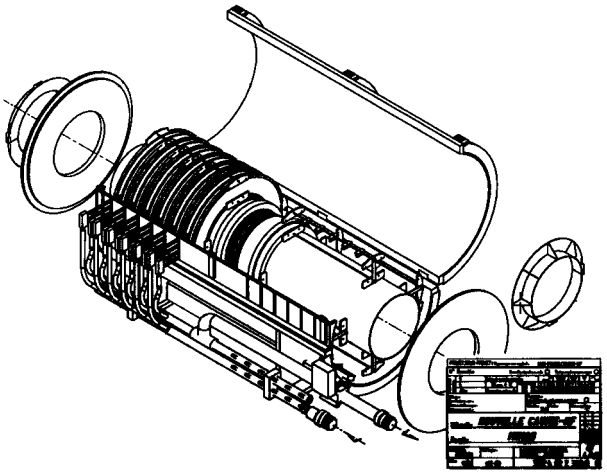

Fig. 30: Cut-away drawing of a VitroVac cavity, showing inner and outer conductor, toroids, and cooling and tuning bars

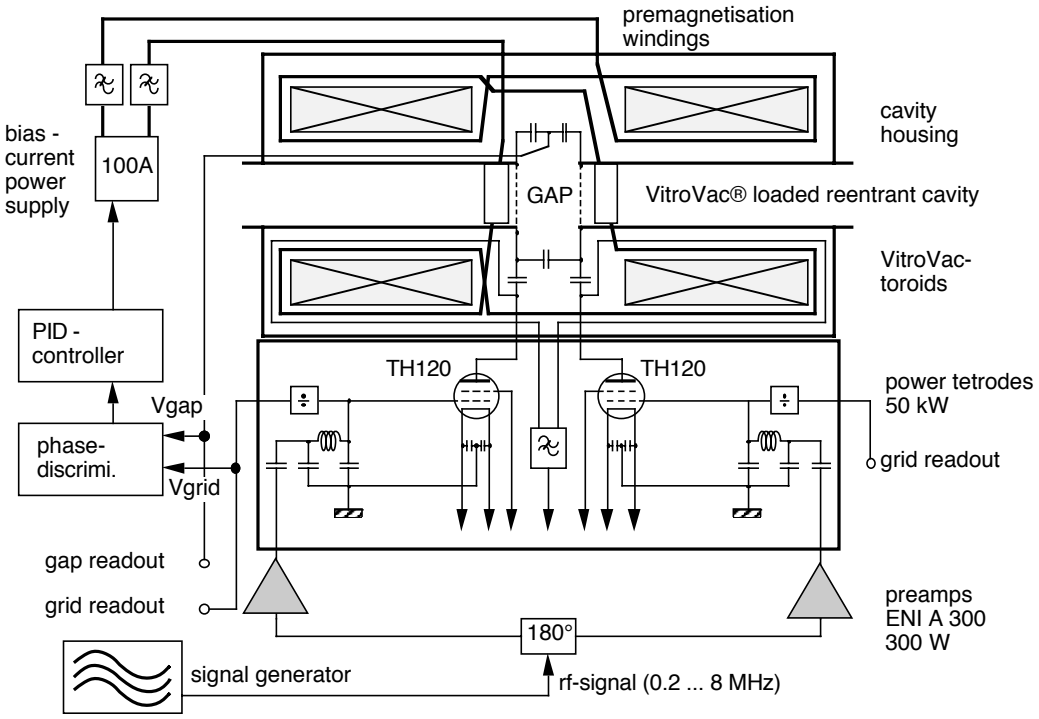

Fig. 31: Layout of the RF system of the VitroVac cavity for operation from 0.2 to 8 MHz

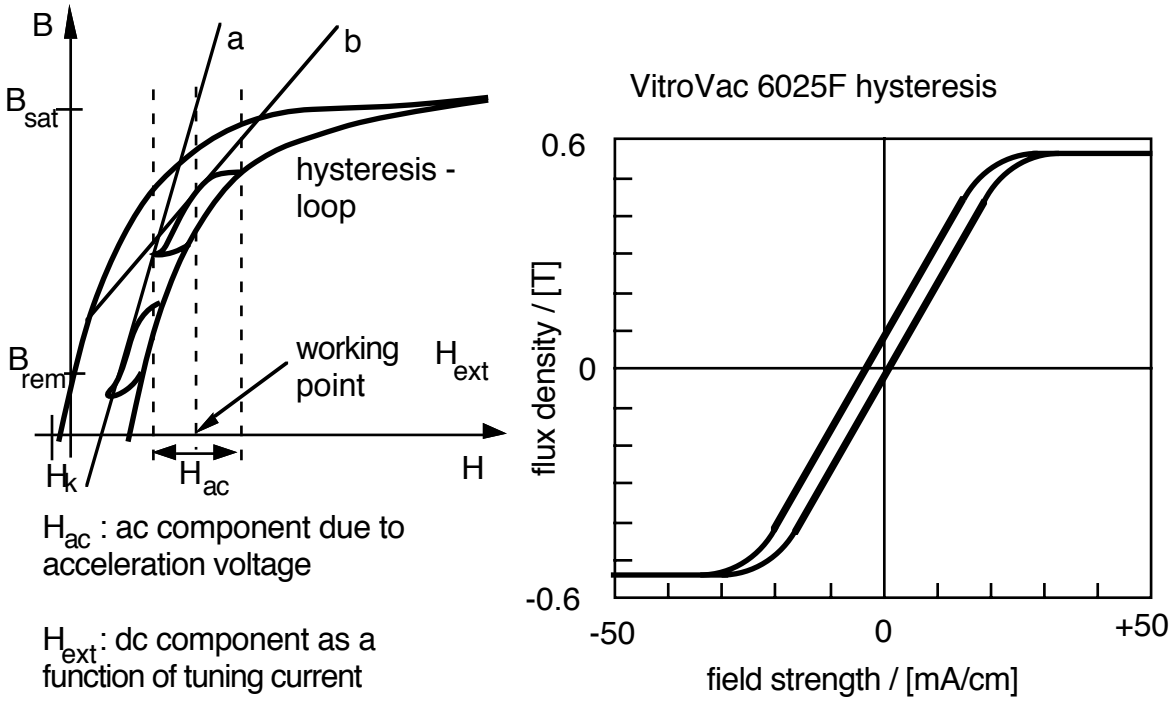

Fig. 32: Hysteresis curve for VitroVac 6025F

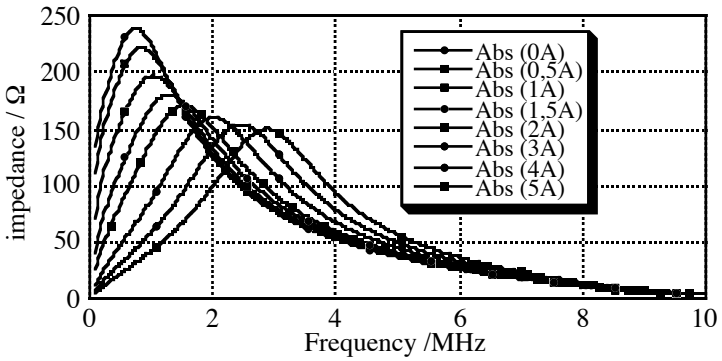

Fig. 33: Absolute value of impedance as a function of frequency and tuning current

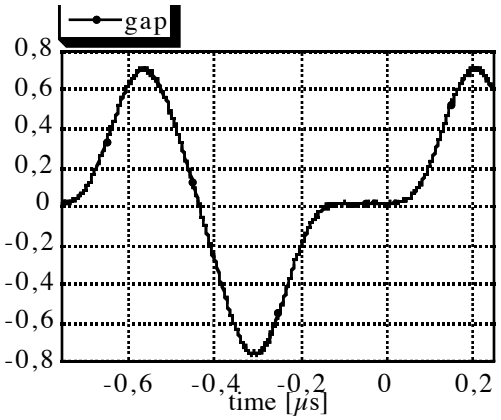

Fig. 34(a): 'Lawn-chair voltage', 0.2 kV; 200 ns per div.

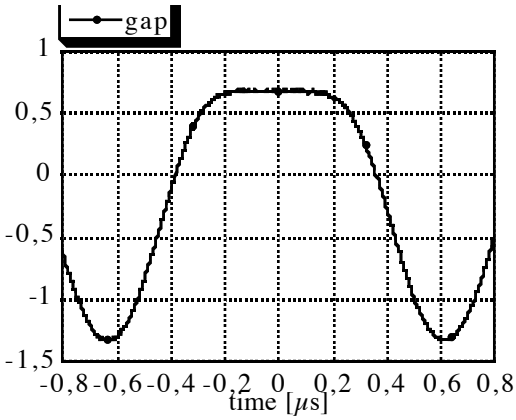

Fig. 32(b): 'Flattened-top voltage', 0.5 kV; 200 ns per div.

The quality of the VitroVac cavity is much lower than the quality of a ferrite cavity. This is shown in Fig. 35, where a 180° phase jump in 20 ns is applied to the cavity. It takes less than three periods to reach a steady state. The same phase jump applied to the COSY ferrite cavity (Fig. 36) shows a much stronger ringing due to the higher quality. Table 2, above, compares some parameters of the VitroVac 6025F-filled cavity with a ferrite 8C12-filled cavity.

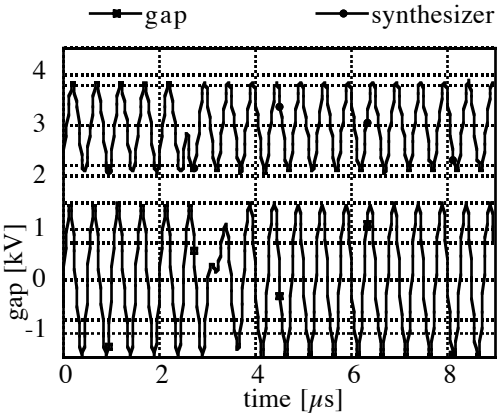

Fig. 35: A rapid 180˚phase jump applied to the VitroVac cavity. Upper trace: synthesizer; lower trace: gap-signal.

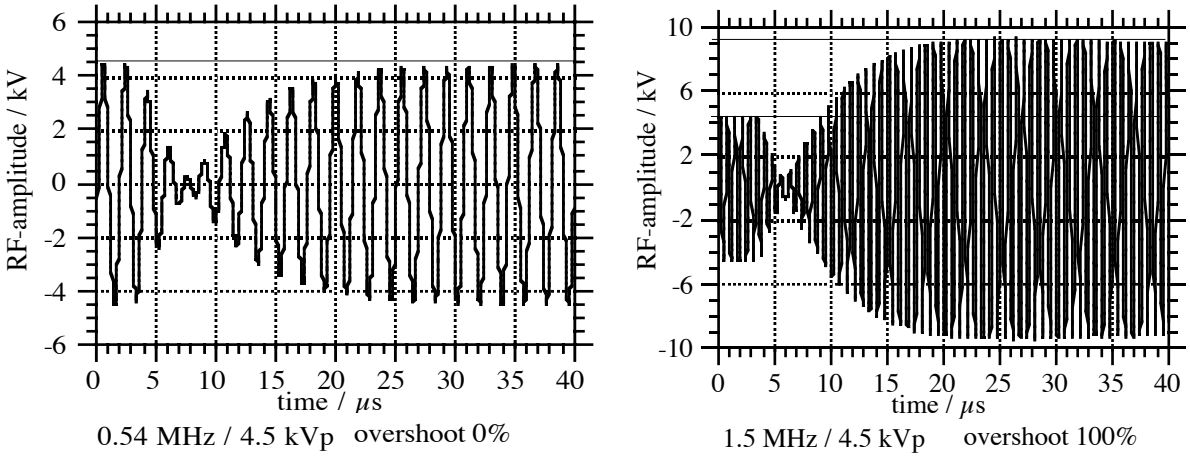

Fig. 36: A rapid 180˚ phase jump applied to an 8C12 ferrite-filled cavity at different frequencies

7.2 Magnetic alloy-filled cavities

In studies for the Japanese Hadron Facility (JHF) [18, 19], NiZn cores were compared with soft magnetic cores made of FineMet. This amorphous material has a very high Curie temperature of about 600°C and allows operation in excess of 100°C. Cores with 67 cm outer diameter and 2.5 cm thickness present an impedance of about 83 Ω. This results in 10 kV/m at 3.4 MHz with 24 cores driven by a 30 kW amplifier.

The broadband behaviour of the impedance of cavities filled with FineMet was clarified in a comparison between cavities for the Barrier Bucket Experiment at AGS, Brookhaven [20, 21]. In the case of ferrite cavities [21], there were eight cells with six cores per cell (one cell reaches 10 kV). In total 80 kV were generated at 3.7 MHz with a 600 kW TH 558 single tetrode amplifier. With the magnetic alloy (MA)-filled cavity [20], a total voltage of 40 kV was obtained with a 60 kW push–pull amplifier.

A cavity filled with high-permeability magnetic alloy was proposed for a high-intensity proton synchrotron [22]. A prototype of only 40 cm in length reached a voltage of 20 kV, which is a gradient of

50 kV/m. Only six cores were used. These were placed directly in a water bath without cooling discs. The prototype and the measured impedance of a half-cavity are plotted in Figs. 37(a) and 37(b). Figure 38 shows the ($\mu'Qf$) product for SY-2 ferrite compared to FineMet FT3 cores. The MA cores exhibit constant shunt impedance up to 2 kG.

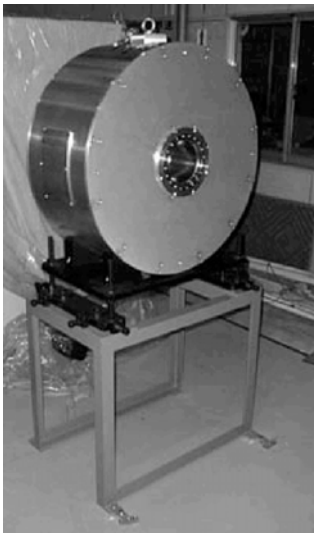

Fig. 37(a): High gradient prototype cavity [23]

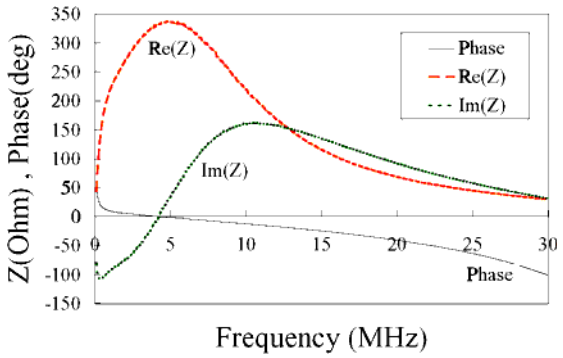

Fig. 37(b): Impedance curve of a half-cavity [22]

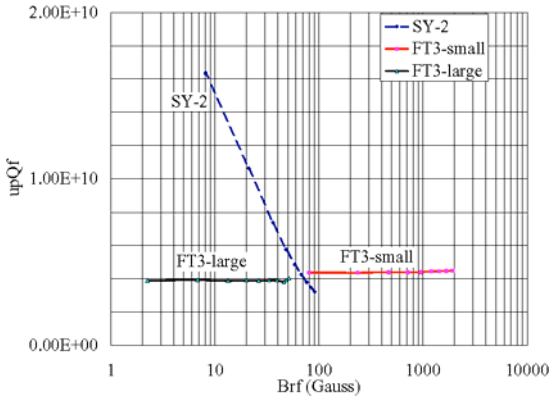

Fig. 38: Dependence of ($\mu'Qf$) values on the RF magnetic field strength (B_{rf}) for Ni Zn ferrite (SY-2) and magnetic alloy (FineMet FT3) cores. FT3-small and -large are cores of 570 mm O.D. and 70 mm O.D. respectively [23].

According to Ref. [23], the characteristics of MA cores can be summarized as follows:

- The ($\mu'Qf$) product of MA cores does not depend on the flux density. Among them, FineMet cores have a large saturation flux density and can be used at the high RF flux density of 2 kG.
- The intrinsic Q-value of the MA core is 0.6–1. It is suitable for a wide frequency sweep without tuning system, barrier bucket, and multiharmonic RF acceleration.
- The permeability of the MA core is about 10 times higher than that of ferrite. Although the Q-value is low, the ($\mu'Qf$) product is high enough to be used for an RF cavity.
- The MA core has a very high Curie temperature of 570°C. The characteristics of the core remain constant at temperatures above 100°C.
- The Q-value of the core can be increased to more than 10 by using the cut core technique. The R/Q-value of the cavity is a variable without changing the shunt impedance.

– The core consists of thin MA tape coated against electrical breakdown by a thin silica insulator. It is possible to manufacture large cores of about 100 cm diameter.

The operation of a High Gradient Cavity (HGC) at HIMAC is described in Ref. [24]. With 60 kW of RF power, a maximum voltage of 4 kV is obtained with a cavity only 40 cm in length. The frequency range is 1–8 MHz; the maximum impedance is 400 Ω between 2–3 MHz.

Another MA-loaded cavity proved the feasibility of barrier-bucket voltages [25]. Because of the high beam current (8 x 10^{12} to 3 x 10^{13}) protons and the broadband behaviour of the cavity, a feedforward system is necessary. The feedforward system has to compensate for the effect whereby the cavity 'talks' to the beam at several harmonics [26]. Some examples of non-sinusoidal waveforms applied to MA-loaded cavities are given in Ref. [27].

7.3 VitroPerm cavity

At COSY, we want to replace the 2.1 m long ferrite cavity (using Philips 8C12) with a much shorter broadband cavity, to gain space for insertions that preserve polarization during acceleration [28]. We have therefore developed the cavity shown in Fig. 39, filled with VitroPerm [29], and which is only about 80 cm long and allows the use of non-sinusoidal waveforms, mentioned above.

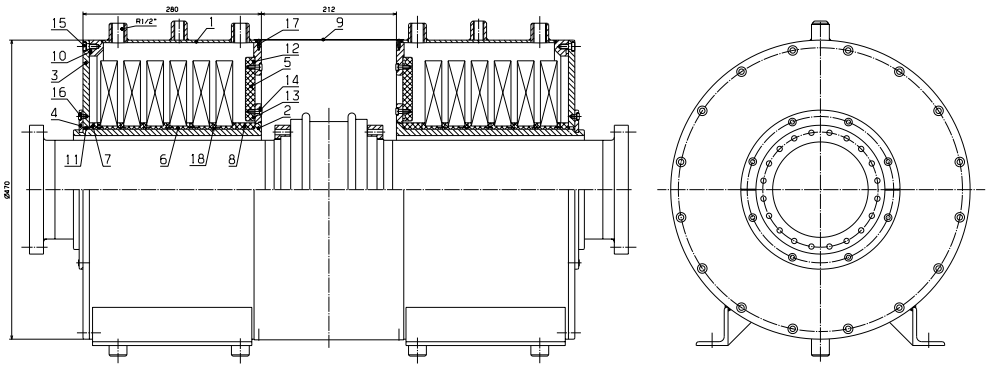

Fig. 39: Layout of a broadband cavity filled with VitroPerm

The parameters of different materials and different cooling media were measured with a small test cavity, shown in Fig. 40 [30]. The measured impedance of a group of three cores as a function of medium is plotted in Fig. 41.

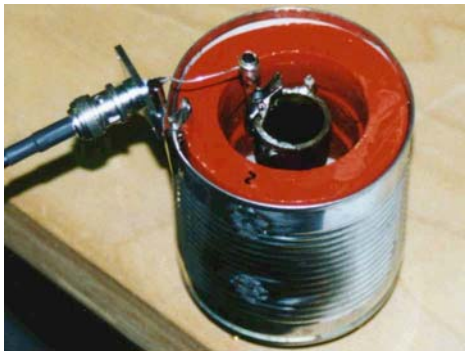

Fig. 40: Small test cavity filled with three cores

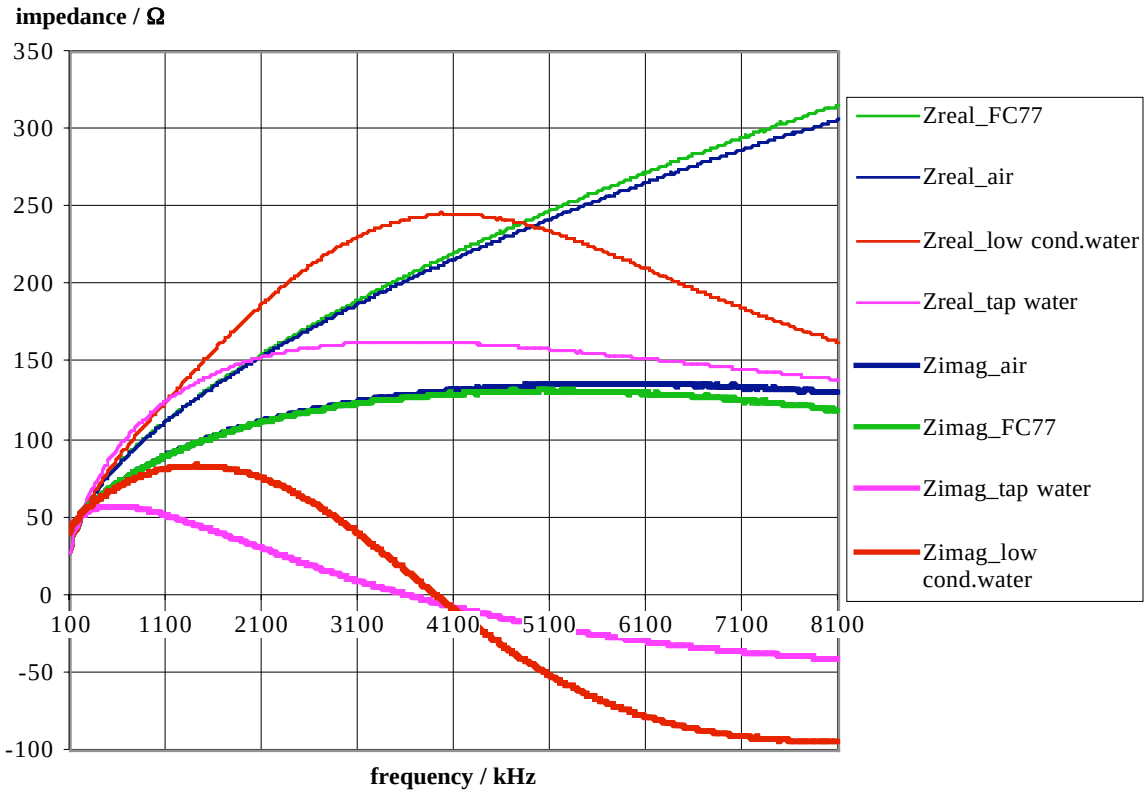

Fig. 41: Impedance of three VitroPerm sample cores as a function of cooling medium

The cooling medium Fluorinert FC_77 [31] with its dielectric constant ε_r = 1.86 leaves the impedance almost untouched compared to air. When using water as a coolant, it is important to use low-conductivity water instead of tap water in order to obtain a high impedance value. The layout of the combination of the VitroPerm-loaded cavity and the tube amplifier is sketched in Fig. 42. The cavity is connected to the amplifier with 200 Ω coaxial transmission lines, shown in Fig. 43. For lower voltages in the kV range, it is sufficient to drive the cavity with a total of four 500 W transistor amplifiers (two per side), connected to (1:4) impedance transformers.

The impedance of the installed air-filled cavity is plotted in Fig. 44. The impedance of the cavity filled with low conductivity water is displayed in Fig. 45. The measurement values for the left and the right half of the cavity are not equal because the value depends on the distribution of the toroids between the left and right sides. Between 500 kHz and 1.6 MHz (the operatimg range of COSY) the total impedance of the cavity is over 500 Ω. An example of the voltages that can be generated with such a cavity, and the reaction of a proton beam at 300 MeV/*c*, are shown in Fig. 46. As expected, this kind of cavity allows modifications of the longitudinal phase space [32].

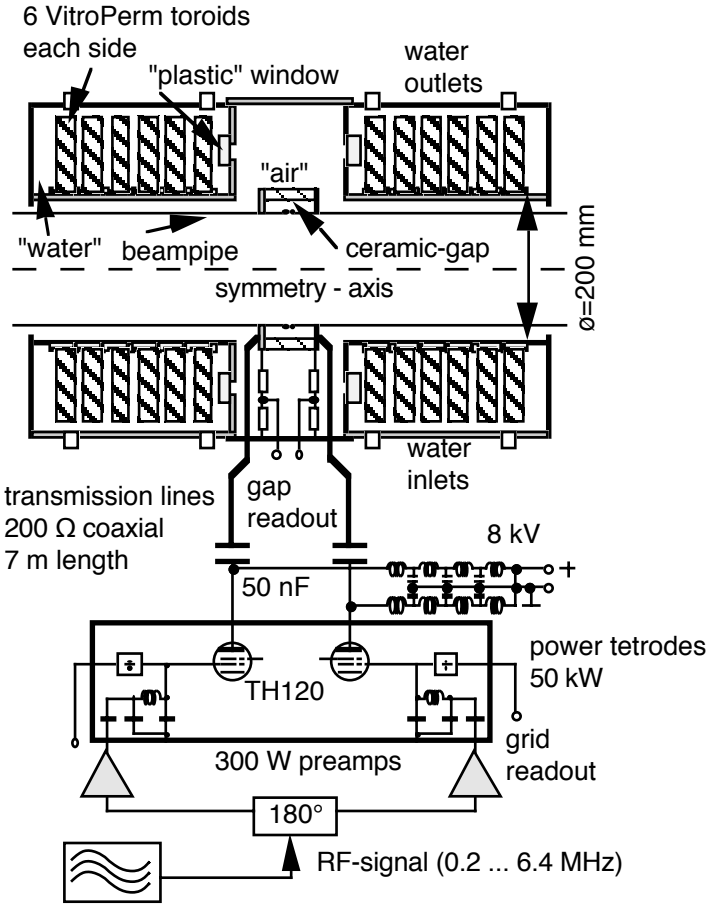

Fig. 42: Combination of VitroPerm cavity and tube amplifier

Fig. 43: Power connection with transmission lines

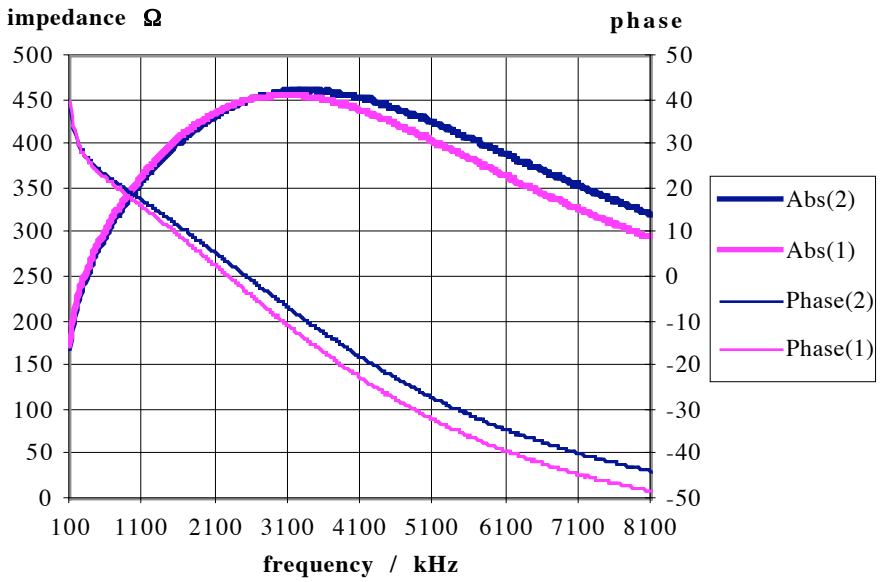

Fig. 44: Impedance of air-filled VitroPerm cavity

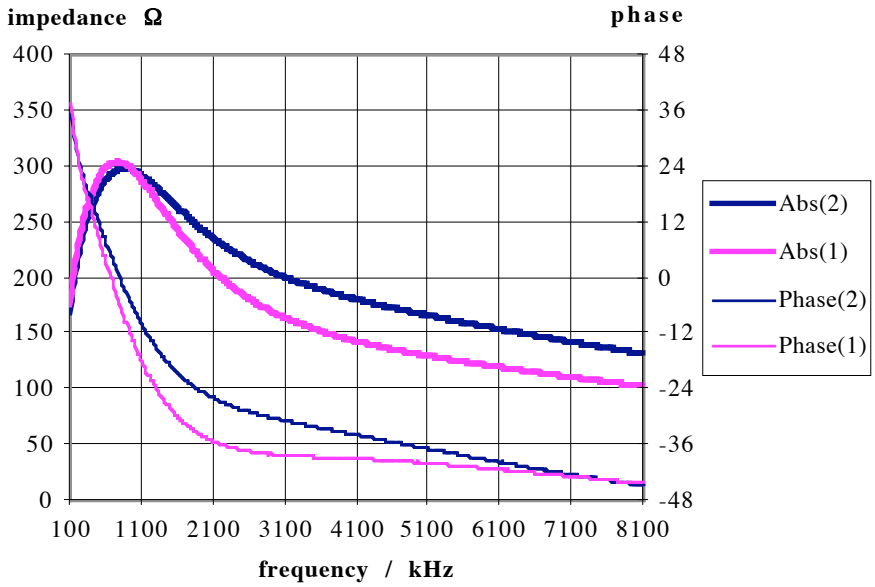

Fig. 45: Impedance of VitroPerm cavity cooled with low-conductivity water

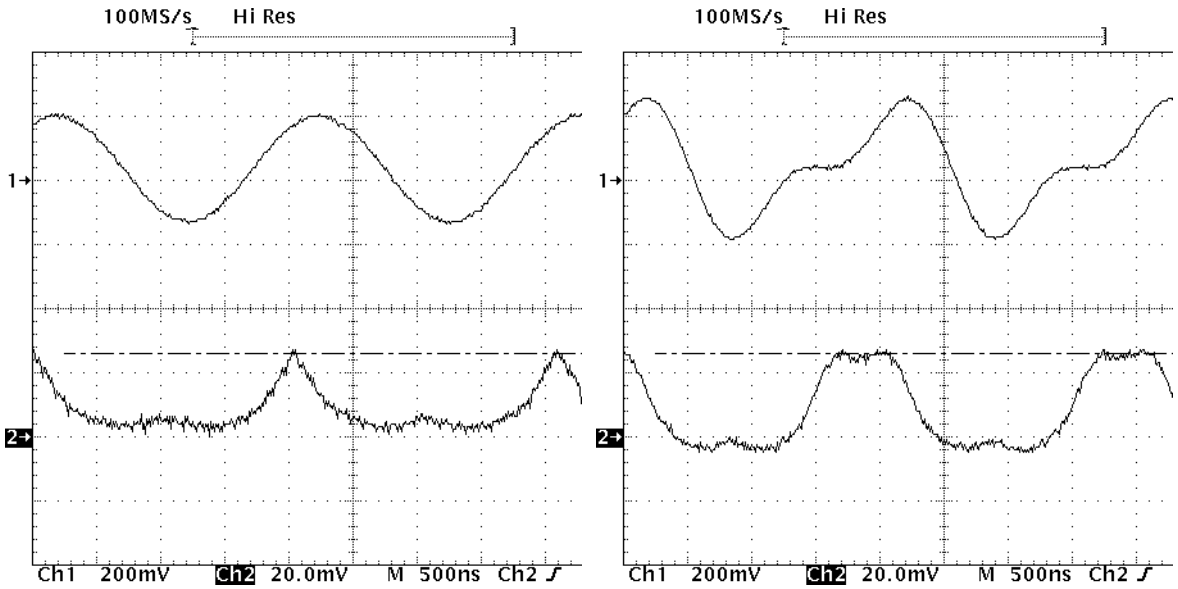

Fig. 46: RF voltage (upper trace) and longitudinal beam signal (lower trace) at COSY injection (500 kHz) with harmonic (h = 1) only (left) and combined harmonics (h = 1) and (h = 2) (right).

REFERENCES

[1] I.S.K. Gardner, Ferrite dominated cavities, 'CERN Accelerator School: RF engineering for particle accelerators', Exeter College, Oxford, 1991, CERN 92–03, CERN, Geneva, 1992.

[2] J. Roberts, *High Frequency Applications of Ferrites* (English Universities Press, 1960).

[3] F.G. Brockman, H. van der Heide and M.W. Louwerse, 'Ferroxcube for proton synchrotrons', Philips Tech. Rev. **30** (1969).

[4] 8C12 Material Grade Specification, Philips Components, 8C12.pdf, December 1999.

[5] P.P. Lombardini, R.R. Schwartz, R.J. Doviak, 'Evaluation of ferrite materials for possible application in the Princeton Pennsylvania 3 BeV proton synchrotron', Moore School Report, No 58-05 (1957).

[6] R.G. Bendall, R.A. Church, 'Ferrite measurements for SNS accelerating cavities', Rutherford Laboratory Report RL-79-04 (1979).

[7] J.E. Griffin, G. Nicholls, 'A review of some dynamic loss properties of NiZn accelerator RF system ferrite', *IEEE Trans. Nucl. Sci.* **NS-26** (1979).

[8] W.R. Smythe, 'Reducing ferrite power loss by bias field rotation', *IEEE Trans. Nucl. Sci.* **NS-30** (1983).

[9] A. Pei, S. Anderson, D. Jenner, X. Kang, S.Y. Lee and D. McCammon, Proc. PAC 97, Vancouver, 1997, p. 2968.

[10] P. Barratt *et al.,* Proc. EPAC-90, Nice, 1990, p. 949.

[11] A. Krusche, M. Paoluzzi, Proc. EPAC 98, Stockholm, 1998, p. 1782.

[12] J.M. Baillod, L. Magnani, G. Nassibian, F. Pedersen, W. Weissflog, 'A second harmonic (6–16 MHz) RF system with feedback-reduced gap impedance for accelerating flat-topped bunches in the CERN PS Booster', Particle Accelerator Conference on Accelerator Engineering and Technology, Santa Fe, 1983 (CERN Report CERN/PS/BR 83–17).

[13] K. Abrahamsson, G. Andler, and C.B. Bigham, A drift tube accelerating structure for CRYRING, *Nucl. Instr. Meth.* **B31** (1988) 475.

[14] J.A. MacLachlan and J.E. Griffin, Proc. IEEE Particle Accelerator Conference, San Francisco, 1991, p. 2826.

[15] K. Abrahamsson *et al.,* Performance of CRYRING with improved electron cooling, Proc. EPAC 94, London, 1994, p. 381.

[16] J.E. Dey and D.W. Wildman, Proc. PAC 99, New York, 1999, p. 869.

[17] P. Ausset, G. Charruau, D. DeMenezes, F.-J. Etzkorn, C. Fougeron, H. Meuth, S. Papureanu, A. Schnase, Proc. EPAC 94, London, 1994, p. 2128.

[18] M. Fujieda, Y. Mori, H. Nakayama, C. Ohmori, S. Sawada, Y. Tanabey, E. Ezura, A. Takagi, M. Toda, M. Yoshii, T. Tanabe, T. Uesugi, Proc. PAC 97, Vancouver, 1997, p. 2992.

[19] C. Ohmori, M. Fujieda, S. Machida, Y. Mori, H. Nakayama, K. Saito, S. Sawada, Y. Tanabe, M. Yamamoto, E. Ezura, A. Takagi, M. Toda, M. Yoshii, T. Tanabe, T. Uesugi, Proc. PAC 97, Vancouver, 1997, p. 2995.

[20] M. Fujieda, S. Machida, Y. Mori, H. Nakayama, C. Ohmori, Y. Sato, Y. Tanabe, T. Uesugi, M. Yamamoto, A. Takagi, M. Toda, M. Yoshii, Y. Iwashita, Proc. EPAC 98, Stockholm, 1998, p. 1796.

[21] M. Yoshii, J.M. Brennan, J. Brodowski, M. Meth, K.A. Rogers, R. Spitz, A. Zaltsman, Proc. EPAC 98, Stockholm, 1998, p. 1829.

[22] Y. Mori, M. Fujieda, K. Koba, H. Nakayama, C. Ohmori, K. Saito, Y. Satoh, Y. Tanabe, A. Takagi, Y. Toda, T. Uesugi, M. Yamamoto, T. Yan, M. Yoshii, Proc. EPAC 98, Stockholm, 1998, p. 299.

[23] C. Ohmori, E. Ezura, M. Fujieda, Y. Mori, R. Muramatsu, H. Nakayama, Y. Sato, A. Takagi, M. Toda, T. Uesugi, M. Yamamoto, M. Yoshii, M. Kanazawa, K. Noda, Proc. PAC 99, New York, 1999, p. 413.

[24] R. Muramatsu, M. Fujieda, Y. Mori, H. Nakayama, C. Ohmori, Y. Sato, A. Takagi, T. Uesugi, M. Yamamoto, M. Yoshii, M. Kanazawa, K. Noda, Proc. PAC 99, New York, 1999, p. 798.

[25] M. Fujieda, Y. Iwashita, A. Noda, Y. Mori, C. Ohmori, Y. Sato, M. Yoshii, M. Blaskiewicz, J.M. Brennan, T. Roser, K.S. Smith, R. Spitz, A. Zaltsmann, Proc. PAC 99, New York, 1999, p. 857.

[26] M. Yamamoto, M. Fujieda, Y. Hashimoto, Y. Mori, R. Muramatsu, C. Ohmori, Y. Sato, A. Takagi, T. Uesugi, M. Yoshii, Proc. PAC 99, New York, 1999, p. 860.

[27] M. Yamamoto, M. Fujieda, Y. Mori, R. Muramatsu, C. Ohmori, Y. Sato, A. Takagi, T. Uesugi, M. Yoshii, M. Kanazawa, K. Noda, Proc. PAC 99, New York, 1999, p. 863.

[28] M. Böhnke, F.-J. Etzkorn, R. Maier, U. Rindfleisch, A. Schnase, H. Stockhorst, Proc. PAC 99, New York, 1999, p. 851.

[29] Vacuumschmelze Hanau GmbH, Kerne und Bauelemente, Datenbuch 1998.

[30] A. Schnase, M. Böhnke, F.-J. Etzkorn, U. Rindfleisch, H. Stockhorst, *IKP Annual Report 1999*, Jül-3744 (Forschungszentrum Jülich GmbH, 2000), p. 150.

[31] 3M, Fluorinert Electronic Liquid FC - 77, Specialty Materials, 3M Center, Building 223-6S-04, St. Paul, MN 55144-1000, USA, see http://www.3m.com/fluids .

[32] H. Stockhorst, *IKP Annual Report 1994,* Jül-3035 (Forschungszentrum Jülich GmbH, 1995), p. 233.

APPENDIX A: THE EFFECTIVE PERMEABIILITY AND THE EFFECTIVE PERMITTIVITY OF A RESONATOR WITH MIXED AIR AND FERRITE FILL

A.1 GENERAL CONSIDERATIONS

It is important to differentiate between resonators in which the ferrite rings are separated from each other by electrically conducting material, like cooling plates, and those separated by an insulator. In the former case very little of the electric field penetrates the ferrite.

A.2 CAPACITANCE PER UNIT LENGTH

Case 1. Ferrite separation by insulator

If we consider a section of the line as in Fig. 9 with a charge (q/m) on the inner conductor then the electric field E at radius r is given by

$$E = \frac{q}{2\pi \varepsilon \varepsilon_0 r}, \tag{A.1}$$

where ε is the permittivity of the material at radius r and ε_0 the permittivity of free space.

The potential V on the inner conductor is given by

$$V = \int_{r_1}^{r_2} E\,dr + \int_{r_2}^{r_3} E\,dr \ , \tag{A.2}$$

where r_1, r_2, and r_3 are the radii of the inner conductor of the co-ax, the inner surface of the ferrite, and the outer surface of the ferrite and the outer conductor respectively.

Then

$$V = \frac{q}{2\pi\,\varepsilon_0}\left(\ln\frac{r_2}{r_1} + \frac{1}{\varepsilon}\ \ln\frac{r_3}{r_2}\right) \ . \tag{A.3}$$

The capacitance per metre is

$$C_t = \frac{2\pi\,\varepsilon_0}{\ln\frac{r_2}{r_1} + \frac{1}{\varepsilon}\ \ln\frac{r_3}{r_2}} = \frac{2\pi\,\varepsilon_e\,\varepsilon_0}{\ln\frac{r_3}{r_1}} \ , \tag{A.4}$$

where ε_e is the effective permittivity of the combined air and ferrite.

Comparing

$$\frac{\varepsilon_e}{\ln\frac{r_3}{r_1}} = \frac{1}{\ln\frac{r_2}{r_1} + \frac{1}{\varepsilon}\ \ln\frac{r_3}{r_2}} \tag{A.5}$$

gives

$$\varepsilon_e = \frac{\varepsilon}{k + \varepsilon\ (1-k)} \ , \text{ where } \ k \ = \ \frac{\ln\frac{r_3}{r_2}}{\ln\frac{r_3}{r_1}} \ . \tag{A.6}$$

Case 2. Ferrite separation by metallic cooling plates

In this case the capacitance per unit length is assumed to be just that of an air-spaced coaxial line with an outer radius r_2. This gives the capacitance C_t :

$$C_t = \frac{2\pi\varepsilon_0}{\ln\frac{r_2}{r_1}} = \frac{2\pi\,\varepsilon_e\,\varepsilon_0}{\ln\frac{r_3}{r_1}} \ . \tag{A.7}$$

From

$$\frac{\varepsilon_e}{\ln\frac{r_3}{r_1}} = \frac{1}{\ln\frac{r_2}{r_1}} \ \text{ and } \ k \ = \ \frac{\ln\frac{r_3}{r_2}}{\ln\frac{r_3}{r_1}} \tag{A.8}$$

follows

$$\varepsilon_e = \frac{1}{1-k} \ . \tag{A.9}$$

A.3 INDUCTANCE PER UNIT LENGTH

For a current i flowing in the coaxial line the inductance per unit length L_t is given by

$$L_t i = \int_{r_1}^{r_3} B\, dr = \int_{r_1}^{r_2} \mu_0 \frac{i}{2\pi r} dr + \int_{r_2}^{r_3} \mu' \mu_0 \frac{i}{2\pi r} dr \tag{A.10}$$

$$L_t = \frac{\mu_0}{2\pi} \left(\ln \frac{r_2}{r_1} + \mu' \ \ln \frac{r_3}{r_2} \right) , \tag{A.11}$$

where B is the magnetic field at radius r, μ_0 is the permeability of free space, and μ' the permeability of the ferrite.

This can be written as

$$L_t = \frac{\mu_e \mu_0}{2\pi} \ \ln \frac{r_3}{r_1} \tag{A.12}$$

where μ_e is the effective permeability of the air and ferrite.

Then

$$\mu_e \ln \frac{r_3}{r_1} = \ln \frac{r_2}{r_1} + \mu' \ \ln \frac{r_3}{r_2} \qquad \mu_e = 1 + k \ (\mu' - 1) \ . \tag{A.13}$$

The values of μ_e and ε_e will be further reduced if there are insulator-filled gaps with $\varepsilon = 1$ and $\mu = 1$ and of thickness d_2 separating the ferrite rings of thickness d_1. The effective values then become

$$\varepsilon_e = \frac{d_1}{d_1 + d_2} \ \frac{\varepsilon}{k + \varepsilon \ (1-k)} \tag{A.14}$$

$$\mu_e = \frac{d_1}{d_1 + d_2} \left(1 + k \ (\mu' - 1)\right) , \tag{A.15}$$

and μ_e remains unaltered by changing the insulator-filled caps to metal-filled gaps.

APPENDIX B: THE CURRENT AND VOLTAGE VARIATION ALONG A RESONATOR

The voltage V and the current i on the transmission line of Fig. 5 are given by the superposition of two waves in opposite directions

$$\begin{aligned} V &= A \cdot e^{j\omega(t - x/v)} + A' \cdot e^{j\omega(t + x/v)} \\ Z_0 i &= A \cdot e^{j\omega(t - x/v)} - A' \cdot e^{j\omega(t + x/v)} \ . \end{aligned} \tag{B.1}$$

The Standing Wave Ratio (SWR) of a line with a short circuit at $x = 0$ is

$$SWR = \frac{0 - Z_0}{0 + Z_0} = -1 \,, \tag{B.2}$$

so the incident and reflected waves have the same magnitude and different sign

$$A' = -A \tag{B.3}$$

$$\begin{aligned} V &= A \cdot e^{j\omega t} \; 2j \sin\frac{\omega x}{v} \\ Z_0 i &= A \cdot e^{j\omega t} \; 2\cos\frac{\omega x}{v} \end{aligned} \,. \tag{B.4}$$

For a complex definition of the voltage $V = V_g\, e^{j\omega t}$ at $x = -l$ the results are

$$A = \frac{-V_g}{2j \sin\frac{\omega l}{v}} \tag{B.5}$$

$$V = -V_g \cdot e^{j\omega t} \; \frac{\sin\frac{\omega x}{v}}{\sin\frac{\omega l}{v}} \tag{B.6}$$

$$i = jV_g \cdot e^{j\omega t} \; \frac{\cos\frac{\omega x}{v}}{Z_0 \sin\frac{\omega l}{v}} \,. \tag{B.7}$$

APPENDIX C: ESTIMATION OF REQUIRED FERRITE QUANTITY

From Section 3.2:

$$B_{rf\,\max} = \mu\mu_0 \; \frac{I}{2\pi \; r_2 \cos\frac{\omega l}{v}} \,, \tag{C.1}$$

and, as I is the current at $x = -l$, then:

$$\begin{aligned} V_g &= I\omega L \\ &= \frac{2\pi r_2 \cdot \cos\frac{\omega l}{v} \; B_{rf\,\max} \cdot Z_0 \tan\frac{\omega l}{v}}{\mu \; \mu_0} \\ &= \frac{r_2 \cdot \ln\frac{r_3}{r_1} \; B_{rf\,\max} \cdot \sin\frac{\omega l}{v} \; \sqrt{\frac{\mu_e}{\varepsilon_e} \; \frac{\mu_0}{\varepsilon_0}}}{\mu \; \mu_0} \,. \end{aligned} \tag{C.2}$$

For $\frac{\omega l}{v} < 26°$, $\sin\frac{\omega l}{v}$ approximates to $\frac{\omega l}{v}$ so that

V_g approximates to

$$V_g = \frac{r_2 \ln \frac{r_3}{r_1} \ \omega B_{rf\ \max} \cdot l \ \ \mu_e}{\mu} . \tag{C.3}$$

Vice-versa l approximates to

$$l = \frac{V_g \ \mu}{\mu_e \ r_2 \ \ln \frac{r_3}{r_1} \ \omega \ B_{rf\ \max}} . \tag{C.4}$$

By choosing B_{rfmax} (typically 0.01 T for NiZn ferrites), an estimate of the total length of ferrite required for an RF system can be made. New materials may achieve higher values of B_{rfmax}.